Coastal and Estuarine Sciences 4

Three-Dimensional Coastal Ocean Models

Norman S. Heaps, Editor

American Geophysical Union
Washington, D.C.
1987

TURBULENT ENERGY CLOSURE SCHEMES

B. Johns

Department of Meteorology, University of Reading, Reading, United Kingdom

T. Oguz

Department of Marine Science, Middle East Technical University, Erdemli, Icel, Turkey

Abstract. A turbulence energy closure scheme is developed for use in three-dimensional models of shelf seas. Applications are described in the modeling of tidal phenomena, wind-driven shallow water over topography and storm surge phenomena. A principal object is to compare the predictions of the modeling procedure with those based on the application of the more frequently used depth-averaged approach.

1. Introduction

The simulation of tidally induced residual flows using numerical models has recently attracted much attention. The motivation for these studies is the recognition that tidal residual circulations are relevant in the coastal marine environment in maintaining the dispersal of pollutants and in other problems concerned with the long-term variability of water masses. In particular, Pingree and Maddock [1977] and Maddock and Pingree [1978] predicted eddies in the residual flow field associated with headlands and reported agreement between observed and computed results for the English Channel.

Using the so-called tidal stress method due to Nihoul and Ronday [1975] in which the linearized solution for the primary tidal motion is used to calculate the forcing terms driving the residual circulation, Ronday [1975] reports a realistic simulation of the residual circulation in the North Sea. Tee [1976] has also described a two-dimensional numerical model for calculating tidally induced residual currents. Further work by Prandle [1978] in estimating the residuals in the Southern Bight of the North Sea due to forcing by the M_2 tide, the mean wind-stress and density gradients suggests that the greatest contribution comes from the tidal asymmetries which must be associated with the nonlinear character of the dynamics. In this work, Prandle used equations for the depth-averaged motion together with a nonlinear empirical representation of the bottom friction. Prandle's conclusion was that the friction term accounts for more than 50% of the nonlinearly supported residual flow; a view supported by our calculations. The way of formulating this term may therefore be crucial.

A possible weakness in these numerical simulation schemes is to be found in their two-dimensional character as well as the highly empirical representation of the bottom friction. The need for a three-dimensional model having a less empirically based frictional representation is therefore apparent. However, with the exception of a model proposed by Durance [1976] and a recent analytical study by Tee [1980] there appears to be little work on the use of three-dimensional models in simulating tidal residuals. Durance employed the technique of Nihoul and Ronday [1975] in order to compute the residual circulation due to tidal asymmetries. The numerical technique used to represent the vertical structure involved the eigenfunction expansion method described by Heaps [1976] which did not therefore require a three-dimensional grid.

Even with a three-dimensional formulation, however, it is necessary to represent appropriately the vertical exchange coefficients in the usual type of gradient transfer law that has been adopted for turbulent momentum fluxes. So much work has used an externally prescribed coefficient that is often taken as a constant. With such an approach, the frictional law is linear and the properties of the turbulent boundary layer at the seafloor will certainly be dependent on the value chosen for the coefficient. Exceptions to be noted are models for oscillatory flows based on the use of a turbulence kinetic energy equation [Vager and Kagan, 1971; Johns, 1978; Leendertsee and Lui, 1978]. It is suggested, therefore, that a model simulation of tidal residuals based on an application of turbulence closure at the level of the energy equation might usefully be compared with one based on the use of the depth-averaged equations.

In this paper we use adaptations of models originally developed by Oguz [1981] for the simu-

lation of the weak tidal and wind-driven circulation in a shallow water basin having the dimensions of the Aegean Sea. The purpose here, however, is not simply to carry out a tuned computer simulation of an observed circulation pattern but to evaluate the consequences of using two conceptually different representations of the frictional mechanism. Accordingly, we use an amplitude for the applied tidal forcing that ensures that the resulting tidal circulation contains an identifiable residual component. Therefore, our experiments relate to the circulation in a now hypothetical basin which is, however, defined by parameters fairly representative of conditions in many shallow sea and shelf regions.

The first model considered is three-dimensional and therefore multilevel with turbulence closure applied at the level of the turbulence energy equation. Similar models have also been developed by, for example, Blumberg and Mellor [1980] and Koutitas and O'Connor [1980]. The second is a vertically integrated model with an empirical representation of the bottom friction. In each of these models the coastal boundaries are represented in a conventional steplike manner by using straight line segments along the coordinate directions. Thus, the model boundaries are characterized by 90° corners which might possibly lead to exaggerated features in the computed residual flow field. Nevertheless, a comparison may then be made between computed tidal and residual quantities determined from two completely different formulations of the dissipative process. Our conclusion is that the three-dimensional and depth-averaged models produce remarkably similar tidal and residual patterns.

The majority of storm surge simulation models are based upon the solution of equations in which the effect of the frictional stress at the seafloor is represented in terms of the depth-averaged current. This procedure, which involves the specification of an empirical friction coefficient, is described, for example, by Reid et al. [1977] and has been extensively used in practical storm surge and tidal calculations by other authors including Heaps [1969], Flather and Heaps [1975], Jelesnianski [1965], and Johns and Ali [1980]. However, even if the bottom stress formulation applied in these works is qualitatively acceptable, the use of a constant friction coefficient might be expected to lead to quantitative shortcomings. This view is supported by calculations carried out by Johns [1978] using a tidal simulation model in which an energy-based turbulence closure scheme is employed to parameterize the Reynolds stress. That study shows that the friction coefficient is strongly dependent on both the local depth and the roughness length of the bottom elements. In a depth-averaged model, failure to incorporate this nonuniformity in a parameterization of the bottom stress may lead to a misrepresentation of the frictional dissipation with the possibility of an erroneous prediction of the surge-induced sea surface elevation.

In this paper, an energy-based turbulence closure scheme is used to parameterize the Reynolds stress in the numerical simulation of wind-driven shallow water flow over an irregular bottom topography. In previous work [Johns, 1978], the tidal flow was driven by a prescribed tidally periodic pressure gradient applied at the seaward end of an elongated channel. There was no applied wind-stress at the free surface of the water. In consequence, almost all the vertical structure in the flow was confined to within 1 m of the floor of the channel. In order to resolve this, a coordinate transformation was used which led to an extremely fine vertical grid-spacing in this intense shear layer. The resolution near the free surface was relatively coarse because of the vertical near-uniformity of the flow in this region. When the flow is driven by the application of a surface wind-stress, however, it is also necessary to resolve the high shears anticipated near the free surface. In this paper a coordinate transformation is applied that meets with this requirement, and a model is developed that may be used to determine the flow structure above an undulation of the seafloor. The numerical model, which has 21 computational levels through the depth, is used to evaluate the effectiveness of the empirically based quadratic bottom friction formulation. In the first experiment, the flow is strictly two-dimensional and the Coriolis acceleration is omitted from the dynamical balance. With a choice of parameters appropriate to a shallow marine environment, a steady state dynamical response is generated by the application of a spatially uniform wind-stress at the sea surface. The velocity structure in a layer of thickness 1 m above the seafloor is found to be well-approximated by a constant stress logarithmic profile. The empirical friction coefficient in the bottom friction law is found to be strongly dependent on the local fluid depth and also on the roughness length of the elements at the seafloor. In applications of this type of frictional representation in storm surge modeling, it is therefore suggested that it may be necessary to formulate an appropriate parameterization of this coefficient. Without this, it seems possible that the frictional dissipation will be misrepresented and that the prediction of surge-induced sea surface elevations will then be in some error.

In the second experiment, the Coriolis effect is included in the dynamical balance although all conditions normal to the direction of the applied surface wind-stress are taken to be uniform. Thus, a transverse current is generated by the geostrophic acceleration and an evaluation can be made of the flow structure beneath a horizontally two-dimensional flow. With regard to the representation of the bottom friction in terms of the dept-averaged current, it is found that there are

now serious qualitative shortcomings in the results.

The numerical simulation of storm surges in the Bay of Bengal has been considered by Johns and Ali [1980] and Johns et al. [1981].

In each of these investigations, the dynamical processes were modeled using depth-averaged equations for the horizontal motion. The modeling approach was therefore similar to that employed by various contributors during the last few years and is well-documented [Nihoul and Ronday, 1976]. The simplifying assumptions made in reducing the fully three-dimensional equations to the conventionally used depth-averaged form are discussed by Johns [1981]. In particular, these relate to the omission of certain nonlinear terms of advective origin in the hydrodynamical equations together with a parameterization of the bottom stress in terms of the depth-averaged motion. In shallow water regions, the omission of these nonlinear terms is strictly justifiable only if there is negligible vertical structure in a fluid column. In the case of storm surge phenomena, this seems unlikely as the momentum supporting the flow is transferred across the sea surface from the atmospheric winds and is communicated to greater depths by vertical turbulent mixing. Thus, we would expect a significant vertical current structure to evolve during this process. The conventional use of an empirically based quadratic friction law involving the depth-averaged current raises further uncertainties as to the viability of the depth-averaged model. This is again because of the occurrence of a disposable friction coefficient that must be assigned a numerical value together with the fact that such a law presupposes that the bottom stress is a function of purely local flow conditions.

The recognition of these potential deficiencies in the depth-averaged approach has led to the development of mathematical techniques based upon the use of the fully three-dimensional equations. For example, Jelesnianski [1970] and Forristall [1974] have investigated the possibility of combining a two-dimensional depth-averaged model (without nonlinear advection) with a locally one-dimensional Ekman model. However, a weakness in this approach is the retention of empirical bottom friction as well as the specification of a constant vertical exchange coefficient. Moreover, the technique of calculating the vertical structure by a local Ekman model may not be valid in shallow water where nonlinear momentum advection is more likely to be significant.

A further contribution to three-dimensional modeling has been made by Nihoul [1977] who also gives a method of combining a depth-averaged and an Ekman model in order to deduce the vertical current structure at each horizontal point. This study is characterized by the prescription of the form of a depth-dependent vertical exchange coefficient. The nonlinear advective terms may be included by an iterative procedure. There is, therefore, a reduced empirical input with reference to the bottom stress although the prescribed form of the vertical exchange coefficient still represents an undesirable element of fairly arbitrary empiricism.

In more recent three-dimensional modeling, Davies [1981] has given a method of solution in which the vertical exchange coefficient may be related to the depth-averaged current, this latter quantity being itself determined from the fully three-dimensional model. This represents a notable advance but it must be emphasized that the method again employs an empirical bottom friction law as part of the seafloor boundary conditions. Work reported by Heaps and Jones [1981] is also characterized by a choice of vertical exchange coefficient dependent upon the bottom stress being given by an empirical quadratic law.

It will therefore be noted that none of these three-dimensional models is sufficiently free from depth-averaged empiricism to provide a comparative assessment of two- and three-dimensional modeling.

Naturally, the final arbiter when deciding upon the merits of different models must be a comparison with a reliable set of observations. Storm surges in the Bay of Bengal have, for obvious reasons, not been monitored by tide gauges with the same precision as, for example, those in the North Sea. However, in Johns et al. [1981], a simulation of the surge generated by the 1977 Andhra cyclone was compared with estimates of flooding that occurred along part of the coast of Andhra Pradesh. In that study, the value chosen for the bottom friction coefficient and the validity of the depth-averaging procedure are far from being uncontentious. Accordingly, in the present chapter we have described a new fully three-dimensional model in order to carry out an independent simulation of the phenomenon. The model is based upon the turbulence energy closure scheme applied by Johns [1978] in a simulation of the tidal flow in a channel. Consequently, the formulation of the frictional mechanism in this new model is conceptually quite different from that used in the depth-averaged approach. Therefore, a meaningful comparison may be made between simulations using two completely independent modeling procedures.

The results of this comparison are at variance with some of our earlier thinking. In this, we had surmised that the shallow water evolution of the surge response would be markedly different in the three-dimensional model because of the full representation of the vertical current structure. Further, we had expected that the sea surface surge response would be critically dependent on the value chosen for the bottom roughness length in the three-dimensional model. Both of these conjectures proved to be incorrect and we found a remarkable qualitative and quantitative similarity between the two simulations. This leads us to conclude that a depth-averaged model may be as effective as a fairly sophisticated

three-dimensional model in storm surge simulation experiments. Therefore, if the vertical current structure is not a primary concern, it may not be worthwhile replacing the depth-averaged procedure by a more complicated technique with its attendant substantial increase in computational overheads.

2. Formulation of a Turbulence Energy Closure Scheme for Three-Dimensional Shelf Models

We use rectangular axes Oxyz where the origin, O, is within the equilibrium level of the sea surface. Conventionally, Ox points towards the east and Oy towards the north. Oz points vertically upwards. The prescribed sea floor topography corresponds to $z = -h(x,y)$ and the displaced level of the sea surface is given by $z = \zeta(x,y,t)$.

Assuming hydrostatic pressure, the equations of motion satisfied by the Reynolds-averaged components of velocity (u,v,w) are

$$\frac{\partial u}{\partial t} + u\frac{\partial u}{\partial x} + v\frac{\partial u}{\partial y} + w\frac{\partial u}{\partial z} - fv = -g\frac{\partial \zeta}{\partial x} + \frac{1}{\rho}\frac{\partial \tau_x}{\partial z} \quad (1)$$

$$\frac{\partial v}{\partial t} + u\frac{\partial v}{\partial x} + v\frac{\partial v}{\partial y} + w\frac{\partial v}{\partial z} + fu = -g\frac{\partial \zeta}{\partial y} + \frac{1}{\rho}\frac{\partial \tau_y}{\partial z} \quad (2)$$

In (1) and (2), f denotes the Coriolis parameter, ρ the density of homogeneous sea water and τ_x and τ_y the components of horizontal Reynolds stress in the x and y directions. We have omitted the direct effect of the astronomical tide generating forces and barometric forcing. Thus, (1) and (2) will only be used to investigate cotidal oscillations in coastal seas and surges generated by wind-stress forcing.

Boundary conditions at an impermeable seafloor relate to an absence of fluid slippage and lead to

$$u = v = w = 0 \quad \text{at } z = -h \quad (3)$$

At the sea-surface, the internal Reynolds stress must equal the applied surface wind-stress $\{\tau_x^\zeta, \tau_y^\zeta\}$. We must therefore have

$$\tau_x = \tau_x^\zeta \qquad \tau_y = \tau_y^\zeta \qquad \text{at } z = \zeta \quad (4)$$

Also, the surface kinematical condition requires that

$$\frac{\partial \zeta}{\partial t} + u\frac{\partial \zeta}{\partial x} + v\frac{\partial \zeta}{\partial y} - w = 0 \quad \text{at } z = \zeta \quad (5)$$

To accompany (1) and (2), the equation of continuity has the vertically integrated form

$$\frac{\partial \zeta}{\partial t} + \frac{\partial}{\partial x}(H\bar{u}) + \frac{\partial}{\partial y}(H\bar{v}) = 0 . \quad (6)$$

In (6), $\bar{u}$ and $\bar{v}$ denote the depth-averaged components of velocity defined by

$$(\bar{u},\bar{v}) = \frac{1}{H}\int_{-h}^{\zeta}(u,v)\,dz \quad (7)$$

where H denotes the total depth, $\zeta + h$.

Equation (1), (2), and (6) do not in themselves constitute a closed set of equations for the determination of u, v, and ζ. Conventionally, closure has been effectively attained by considering two-dimensional depth-averaged versions of (1) and (2). The bottom stress,

$$(\tau_x^{-h}, \tau_y^{-h})$$

is then related to the depth-averaged velocity by an empirically based friction law containing a disposable friction coefficient, C_f. In the case of quadratic bottom friction, this has the form

$$(\tau_x^{-h}, \tau_y^{-h}) = C_f \rho (\bar{u}^2 + \bar{v}^2)^{1/2}(\bar{u},\bar{v}) \quad (8)$$

In this chapter, we introduce a vertical exchange coefficient, K, and write

$$\tau_x = K\rho\,\partial u/\partial z \qquad \tau_y = K\rho\,\partial v/\partial z \quad (9)$$

Following Johns [1978], this coefficient is related to the turbulence energy density, E, by

$$K = c^{1/4}\,\ell\,E^{1/2} \quad (10)$$

The constant, c, is recommended by Launder and Spalding [1972] as 0.08 and the length scale, ℓ, of the vertical mixing process is determined from the local similarity law

$$\ell = -\frac{\kappa E^{1/2}\ell^{-1}}{(\partial/\partial z)(E^{1/2}\ell^{-1})} \qquad \ell = \kappa z_0 \text{ at } z = -h \quad (11)$$

In (11), κ is von Karman's constant (taken as 0.4) and z_0 is the roughness length of elements at the seafloor. The turbulence energy density satisfies a transport equation simulating the ways in which turbulence is generated, redistributed and dissipated. This has the form

$$\frac{\partial E}{\partial t} + u\frac{\partial E}{\partial x} + v\frac{\partial E}{\partial y} + w\frac{\partial E}{\partial z} = K\left\{\left(\frac{\partial u}{\partial z}\right)^2 + \left(\frac{\partial v}{\partial z}\right)^2\right\} + \frac{\partial}{\partial z}\left(K\frac{\partial E}{\partial z}\right) - \varepsilon \quad (12)$$

The first term on the right-hand side of (12) represents the effect of turbulence generation by energy extraction from the Reynolds-averaged flow. The second term represents a vertical redistribution of turbulence energy which is assumed to follow a gradient transfer law with the same

exchange coefficient as that for momentum exchange. The final term, ϵ, represents a dissipative effect. Some authors [e.g., Marchuk et al., 1977] have considered a turbulence decay equation to determine ϵ but here we follow Johns [1978] and Leendertsee and Liu [1978] and use a similarity relation in which ϵ is parameterized according to

$$\epsilon = c^{3/4} E^{3/2}/\ell \qquad (13)$$

Additional boundary conditions to accompany (12) relate to an assumed absence of turbulence energy transfer across the seafloor and the sea surface. These lead to

$$\begin{aligned} \partial E/\partial z &= 0 \quad \text{at } z = -h \\ \partial E/\partial z &= 0 \quad \text{at } z = \zeta \end{aligned} \qquad (14)$$

For physical realism, (14) requires the existence of surface and bottom layers through which E is constant. For the bottom layer, this is equivalent to there being a constant stress layer.

In our applications of the equations developed in the preceding paragraphs, it is convenient to make use of a new vertical coordinate, σ, defined by

$$\sigma = \frac{z + h}{H} \qquad (15)$$

Thus, the seafloor and sea surface correspond respectively to $\sigma = 0$ and $\sigma = 1$. Such a coordinate appears to have been introduced into oceanography by Freeman et al. [1972] although an analogous coordinate has had a distinguished history in meteorology and was introduced by Phillips [1957]. Taking, x, y, σ, and t as new independent variables, and introducing into (1) and (2) the parameterization (9), the components of velocity are readily shown to satisfy

$$\frac{\partial \tilde{u}}{\partial t} + \frac{\partial}{\partial x}(u\tilde{u}) + \frac{\partial}{\partial y}(v\tilde{u}) + \frac{\partial}{\partial \sigma}(\omega\tilde{u}) - f\tilde{v} = -gH\frac{\partial \zeta}{\partial x} + \frac{1}{H^2}\frac{\partial}{\partial \sigma}\left(K\frac{\partial \tilde{u}}{\partial \sigma}\right) \qquad (16)$$

and

$$\frac{\partial \tilde{v}}{\partial t} + \frac{\partial}{\partial x}(u\tilde{v}) + \frac{\partial}{\partial y}(v\tilde{v}) + \frac{\partial}{\partial \sigma}(\omega\tilde{v}) - f\tilde{u} = -gH\frac{\partial \zeta}{\partial y} + \frac{1}{H^2}\frac{\partial}{\partial \sigma}\left(K\frac{\partial \tilde{v}}{\partial \sigma}\right) \qquad (17)$$

where

$$\tilde{u} = Hu \qquad (18)$$

$$\tilde{v} = Hv$$

$$\omega = \frac{\partial \sigma}{\partial t} + u\frac{\partial \sigma}{\partial x} + v\frac{\partial \sigma}{\partial y} + w\frac{\partial \sigma}{\partial z} \qquad (19)$$

The turbulence energy density satisfies

$$\frac{\partial \tilde{E}}{\partial t} + \frac{\partial}{\partial x}(u\tilde{E}) + \frac{\partial}{\partial y}(v\tilde{E}) + \frac{\partial}{\partial \sigma}(\omega\tilde{E}) = \frac{K}{H^3}\left\{\left(\frac{\partial \tilde{u}}{\partial \sigma}\right)^2 + \left(\frac{\partial v}{\partial \sigma}\right)^2\right\} + \frac{1}{H^2}\frac{\partial}{\partial \sigma}\left(K\frac{\partial \tilde{E}}{\partial \sigma}\right) - H\epsilon \qquad (20)$$

where

$$\tilde{E} = HE \qquad (21)$$

Depth-averaged components of velocity defined by (7) are then given by

$$(\bar{u}, \bar{v}) = \int_0^1 (u, v)\, d\sigma \qquad (22)$$

Following Johns [1978], ω is readily found to satisfy the diagnostic equation

$$\frac{\partial}{\partial x}\left[H(u - \bar{u})\right] + \frac{\partial}{\partial y}\left[H(v - \bar{v})\right] + \frac{\partial}{\partial \sigma}(H\omega) = 0 \qquad (23)$$

The seafloor conditions (3) are equivalent to

$$u = v = \omega = 0 \quad \text{at } \sigma = 0 \qquad (24)$$

and the sea surface conditions (4), when combined with (9), lead to

$$K\frac{\partial u}{\partial \sigma} = \frac{H\tau_x^{\zeta}}{\rho} \qquad K\frac{\partial v}{\partial \sigma} = \frac{H\tau_y^{\zeta}}{\rho} \qquad \text{at } \sigma = 1 \qquad (25)$$

The kinematical condition (5) is equivalent to

$$\omega = 0 \quad \text{at} \quad \sigma = 1 \qquad (26)$$

and the energy condition (14) is satisfied provided that

$$\frac{\partial E}{\partial \sigma} = 0 \quad \text{at } \sigma = 0 \text{ and } \sigma = 1 \qquad (27)$$

Before applying these equations to a specific problem, additional lateral boundary conditions are required. These may either relate to the requirement that there be no volume flux of water across a coastline or that there are prescribed dynamical conditions at open-sea boundaries. These will be developed as and where necessary.

3. Application to the Modeling of the Tidally Induced Residual Circulation in a Shallow Basin

In this section, our principal object is to model a tidally induced residual circulation pattern by using the three-dimensional formulation of the dynamics and to compare this with an evaluation based on the depth-averaged procedure.

The depth-averaged equations are readily obtained by the vertical integration of (16) and (17) between the seafloor and the sea surface. With the neglect of the applied surface wind stress, this procedure leads to equations of the form

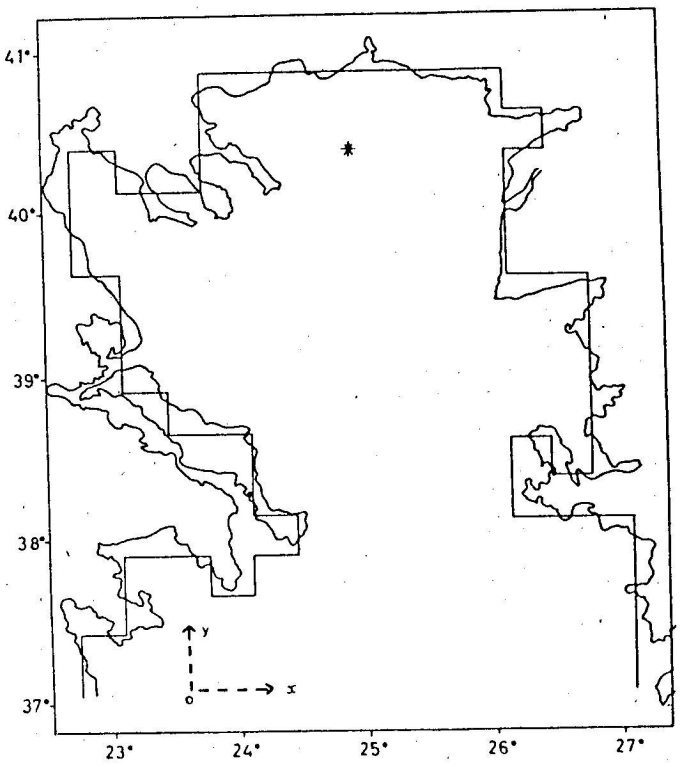

Fig. 1. The model analysis area.

$$\frac{\partial}{\partial t}(H\bar{u}) + \frac{\partial}{\partial x}(H\bar{u}^2) + \frac{\partial}{\partial y}(H\bar{\bar{u}}\bar{\bar{v}}) + \frac{\partial}{\partial x} H(\overline{u^2} - \bar{\bar{u}}^2) + \frac{\partial}{\partial y} H(\overline{\bar{u}\bar{v}} - \bar{\bar{u}}\bar{\bar{v}}) - fH\bar{v} = -gH\frac{\partial \zeta}{\partial x} - \frac{\tau_x^{-h}}{\rho} \quad (28)$$

and

$$\frac{\partial}{\partial t}(H\bar{v}) + \frac{\partial}{\partial x}(H\bar{\bar{u}}\bar{\bar{v}}) + \frac{\partial}{\partial y}(H\bar{v}^2) + \frac{\partial}{\partial x} H(\overline{\bar{u}\bar{v}} - \bar{\bar{u}}\bar{\bar{v}}) + \frac{\partial}{\partial y} H(\overline{v^2} - \bar{\bar{v}}^2) + fH\bar{u} = -gH\frac{\partial \zeta}{\partial y} - \frac{\tau_y^{-h}}{\rho} \quad (29)$$

In (28) and (29), the overbars denote the depth-averaged value of quantities and the bottom stress terms are parameterized by use of (8).

Numerical experiments carried out by Johns [1978] using the turbulence energy closure scheme have indicated that

$$\bar{\bar{u}}^2/\overline{u^2} < 1.04$$

This supports the neglect of the vertical structure correction terms in (28) and (29) and implies the existence of a relatively thin bottom boundary layer. With this simplification, (28) and (29) then reduce to

$$\frac{\partial}{\partial t}(H\bar{u}) + \frac{\partial}{\partial x}(H\bar{u}^2) + \frac{\partial}{\partial y}(H\bar{\bar{u}}\bar{\bar{v}}) - fH\bar{v} = -gH\frac{\partial \zeta}{\partial x} - C_f \bar{u}(\bar{u}^2 + \bar{v}^2)^{1/2} \quad (30)$$

and

$$\frac{\partial}{\partial t}(H\bar{v}) + \frac{\partial}{\partial x}(H\bar{\bar{u}}\bar{\bar{v}}) + \frac{\partial}{\partial y}(H\bar{v}^2) + fH\bar{u} = -gH\frac{\partial \zeta}{\partial y} - C_f \bar{v}(\bar{u}^2 + \bar{v}^2)^{1/2} \quad (31)$$

We apply the equations based on the three-dimensional model (referred to as MLM) and those based on the depth-averaged model (referred to as VIM) to a calculation of the tidal circulation induced in an idealized shallow water basin depicted in Figure 1. In each of these models, the coastal boundaries are represented in a conventional steplike manner by using straight line segments along the coordinate directions. Thus, the model boundaries are characterized by 90° corners which might possibly lead to exaggerated features in the computed tidal residual flow field. Nevertheless, a comparison may then be made between computed tidal and residual quantities determined from two completely different formulations of the dissipative mechanism.

A forcing condition is applied at the open-sea boundary in the form

$$\bar{v} + \left(\frac{g}{h}\right)^{1/2} \zeta = 2a\left(\frac{g}{h}\right)^{1/2} \sin\left(\frac{2\pi t}{T}\right) \quad (32)$$

In (32), a is the amplitude of the forting harmonic and T is its period. An oscillatory response is established in the usual way by integrating the equations ahead in time from an initial state of rest. The solution becomes effectively oscillatory after about 10 tidal cycles of integration as a result of the frictional dissipation of the transient response. The specification of the tidal forcing in the form of the radiation condition (32) has the advantage that the initially generated transients tend to be transmitted across the open-sea boundary and out of the analysis area. Such a condition has been found useful in work reported by Johns et al. [1981, 1983].

In MLM equations (16) through (23) are replaced by finite-difference analogues relating the prognostic variables at time $t + \Delta t$ to their values at time t. The vertical coordinate, σ, is discretized according to the procedure described by Johns [1978] in which there is a grid refinement adjacent to $\sigma = 0$ leading to a fine resolution near the floor of the basin in comparison with the mid-depths. An idealized bathymetry is taken in which the depth of the water decreases from about 100 m in the deepest parts of the basin in the south to about 30 m near the coastline. The height of the first computational level above the

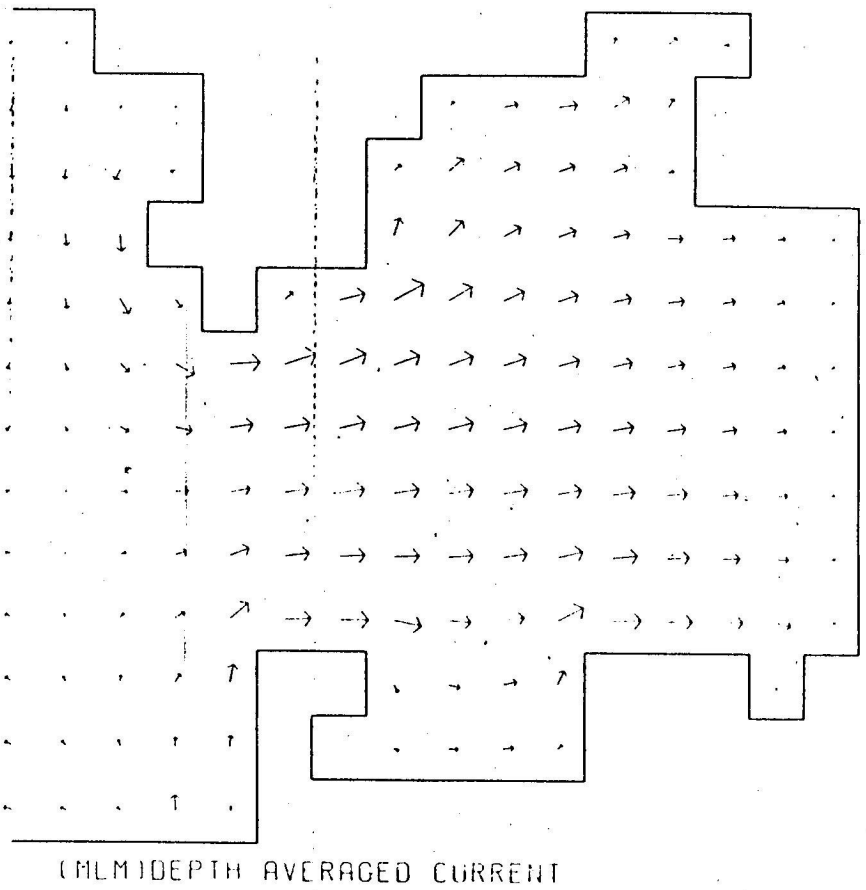

Fig. 2a. Depth-averaged current vectors at t = (0.5)T calculated from MLM.

floor then varies between about 3.8 cm and 12.7 cm. The roughness length of the bottom elements is taken to be 1 cm.

The horizontal coordinates are discretized so that the space increment in both coordinate directions is 14 km. The computation of updated values of ζ, u, and v is performed on a staggered grid consisting of three distinct types of grid-point at each of which only one of the three prognostic variables is carried. The prognostic energy variable, E, is carried at the same grid-points as ζ. The use of this type of scheme in a storm surge modeling context is described, for example, by Johns et al. [1981].

The discretization of the equations in VIM uses the same horizontal grid as that of MLM. The bathymetry is also the same and, unless otherwise stated, we use a spatially and temporally uniform standard value of C_f equal to 2.6×10^{-3}. In both models, the value of the Coriolis parameter is 10^{-4} s^{-1}, a is 1.0 m and T is 12.4 hr. The numerical time-stepping procedure uses 300 time steps per tidal cycle.

In Figures 2a and 2b we give the depth-averaged current vector pattern at t = (0.5)T calculated from MLM and VIM respectively. Both qualitatively and quantitatively, the difference between these is almost imperceptible. The maximum tidal currents in the basin are of order 0.5 m s^{-1} and we find that the direction of the near-bottom and surface current differs by not more than about 10° during the tidal cycle. Presumably, this is one reason why the VIM circulation compares so well with that computed from MLM for this shallow sea region.

Further appraisal of the predictions of VIM requires a grid-point analysis of the tidal variations during a cycle in each of the two models. In Figure 3 we give the variations of ζ, u, and v from both MLM and VIM at a representative position indicated with an asterisk in Figure 1. As is clearly seen, the variations of these quantities during a tidal cycle are remarkably similar. The small phase differences are attributed to the use of the quadratic law in VIM compared with the gradient transfer law for momentum exchange in MLM. These results, which differ by no more than a maximum of 10% anywhere in the

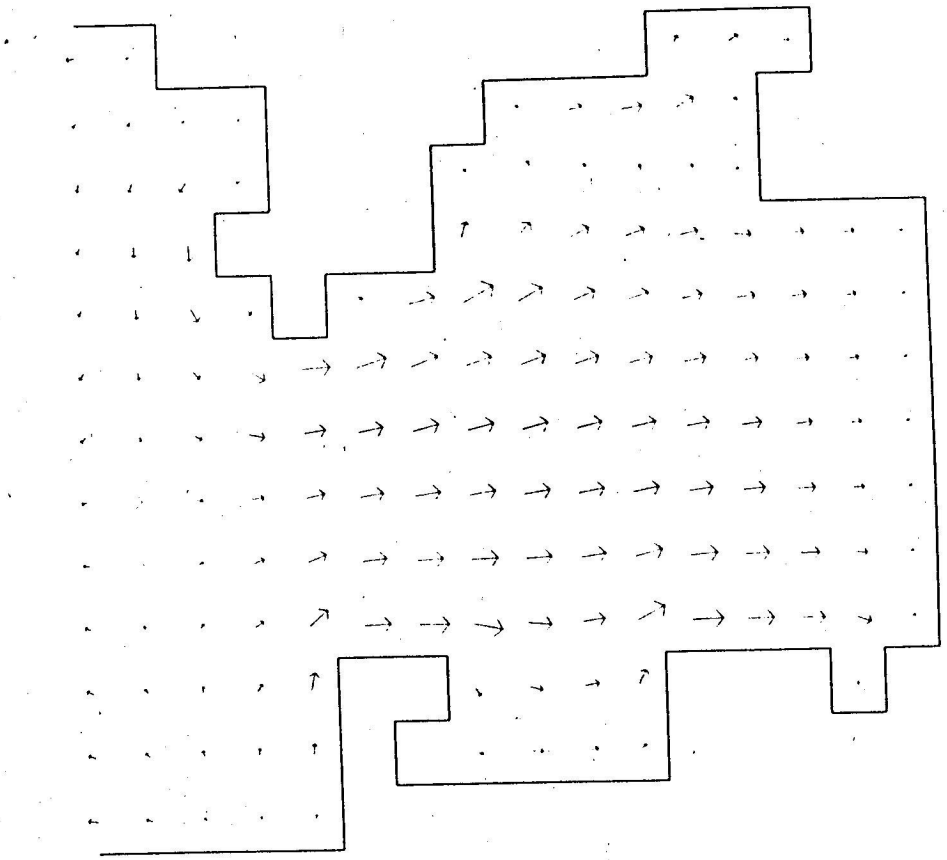

(VIM) HORIZONTAL CURRENT

Fig. 2b. Same as Figure 2a, except calculated from VIM.

basin therefore strongly support the use of VIM if the vertical variation of the currents in the bottom boundary layer is not the main interest.

The close agreement between the calculations of ζ, u, and v based on MLM and VIM suggests that the empirical quadratic law may yield a good representation of the bottom stress with much less computation than is required in the energy-based closure model. This conjecture may be appraised directly by calculating the tidal variation of the bottom stress, τ_b, separately from MLM and VIM. In Figure 4, we give the variation of $|\tau_b|/\rho$ during the tidal cycle at the marked position in the basin. For MLM, this is calculated from

$$|\tau_b|/\rho = c^{l/2} E_b \qquad (33)$$

where E_b is the bottom turbulence energy density. The direction must be determined by evaluation of (9) at $z = -h$.

For VIM, we use

$$|\tau_b|/\rho = C_f (\bar{u}^2 + \bar{v}^2) \qquad (34)$$

with the standard value of C_f.

We note that the quadratic law underestimates $|\tau_b|$, especially so for the peak values when the underestimate can amount to 40%. The predicted phase of the bottom stress is seen to be almost identical in each of the model calculations.

In summary, then, it appears that VIM with $C_f = 2.6 \times 10^{-3}$ is almost equivalent to MLM as far as the predictions of ζ, u, and v are concerned. However, if it is the bottom stress that is of primary importance (as in sedimentation studies), VIM will tend to underpredict using the standard value of C_f. It is informative, therefore, to deduce an appropriate value of C_f from MLM and then to use this in VIM in order to see how the computed stress and other tidal quantities are affected. The derived value of C_f is of course both spatially and temporally variable. However, as in Johns [1978], we may define an optimized and temporally invariant value by

$$C_f = \frac{\int_0^T |\tau_b|/\rho \, (\bar{u}^2 + \bar{v}^2)\, dt}{\int_0^T (\bar{u}^2 + \bar{v}^2)^2 dt} \qquad (35)$$

where all the quantities are evaluated from MLM.

We find that (35) leads to a value of C_f that is higher than the standard value and which has a

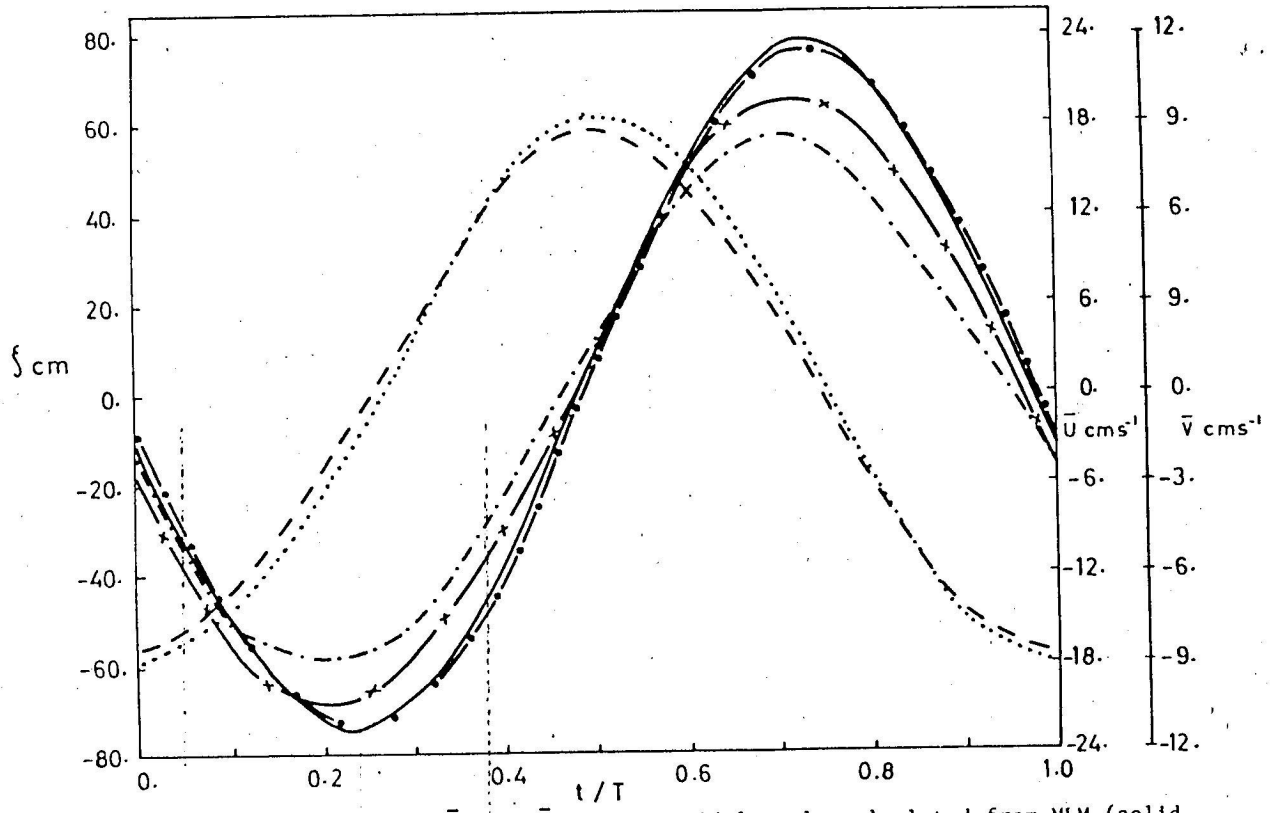

Fig. 3. Variations of ζ, $\bar{u}$, and $\bar{v}$ during a tidal cycle calculated from MLM (solid curve, ζ; dashed curve $\bar{u}$; dot-dashed curve, $\bar{v}$) and VIM (heavy dot-dashed curve, ζ; dotted curve, $\bar{u}$; cross-dashed curve, $\bar{v}$).

spatial average of about 5×10^{-3}. This value was then used in VIM to compute the bottom stress and the resulting variation of $|\tau_b|/\rho$ during a tidal cycle is also shown in Figure 4. From this, we note that the bottom stress is brought into much closer agreement with that calculated from MLM although the peak values now occur slightly later than in MLM.

The effect on the elevation of the use of an increased value of C_f in VIM is far less marked and leads to only a slight improvement in this already relatively well-predicted quantity. It is therefore inferred that VIM is only weakly dependent on the value of the friction coefficient as far as the tidal variation of ζ is concerned. If it is the bottom stress that is required, then the input value of C_f is of critical importance when using VIM in a predictive capacity.

During the final cycle of integration, the time averages of $\bar{u}$ and $\bar{v}$ have been calculated from

$$(\langle\bar{u}\rangle, \langle\bar{v}\rangle) = \frac{1}{T}\int_0^T (\bar{u},\bar{v})\, dt \qquad (36)$$

We then determined the implied residual flow field using both MLM and VIM with the standard value of C_f and these are shown respectively in Figures 5a and 5b. In each case, the maximum residual current velocity is about 3 cm s^{-1} and, quantitatively and qualitatively, the different models yield virtually identical patterns. We note the cellular structures which are seen to be associated with the stepwise treatment of the coastal boundaries. Caution is required in the interpretation of these when the model coastline is in fact an approximation to a smoother real feature as there is strong evidence that they do not occur in models with a more natural curvilinear treatment of the boundaries [Oguz, 1981].

An analysis of the depth-structure of the residual field derived from MLM shows that the residual current increases rapidly from zero at the floor of the basin to an asymptotic value above a bottom boundary layer having a scale thickness of about 1 m. The direction does not change significantly in this vertical variation thus leading to an almost unidirectional current through the depth of the water. There is, therefore, no veering through the depth because of the confinement of all vertical structure to a relatively thin bottom boundary layer.

There is, of course, no closed streamline pattern for the depth-averaged residual current field. The residual current is a horizontally divergent quantity and continuity in the residual circulation is maintained through the nondiver-

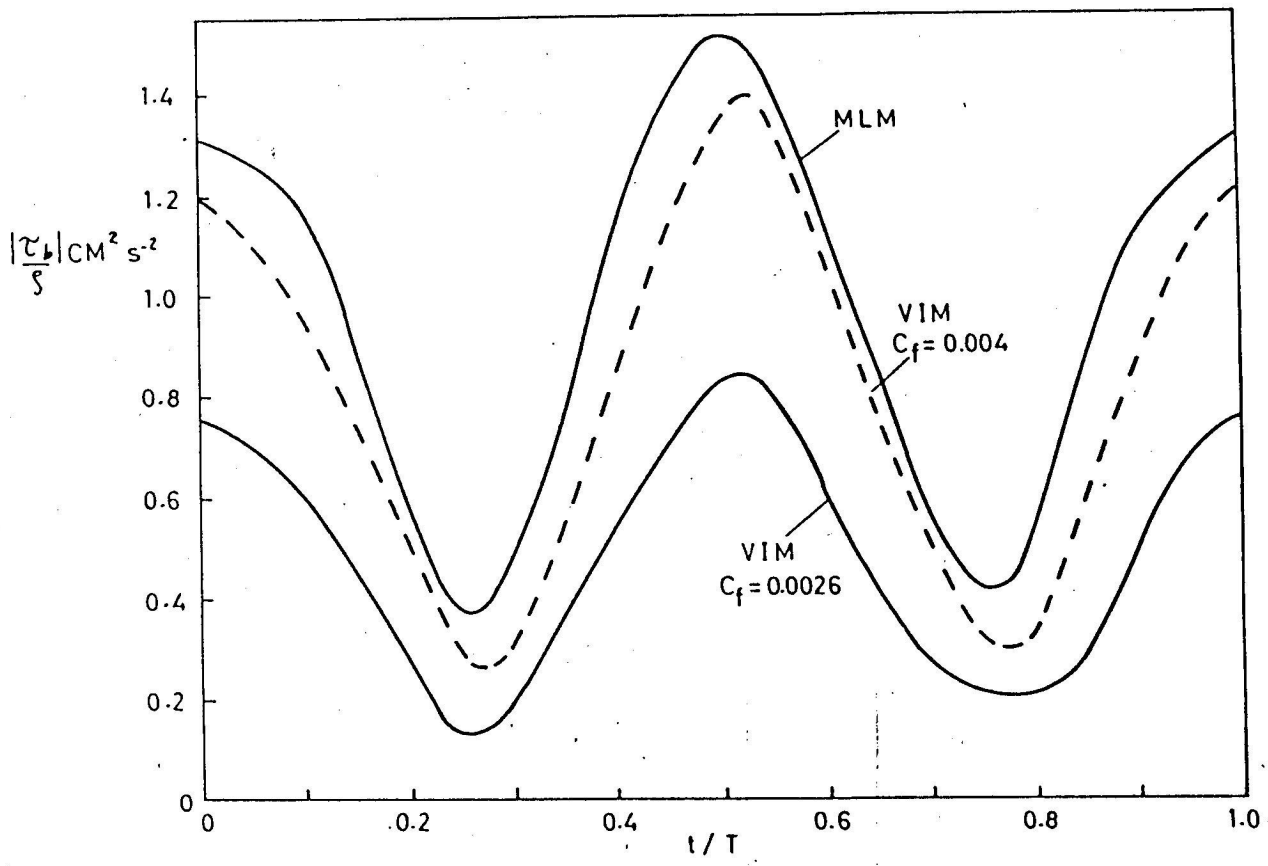

Fig. 4. Variation of $|\tau_b|/\rho$ during a tidal cycle calculated from MLM and VIM.

gence of the residual mass transport field. From (6) this is equivalent to

$$\frac{\partial}{\partial x} \langle(\zeta + h)\bar{u}\rangle + \frac{\partial}{\partial y} \langle(\zeta + h)\bar{v}\rangle = 0 \qquad (37)$$

The integration of (37) over the entire basin yields

$$\int_B \langle(\zeta + h)\bar{u}\rangle \, dy = 0 \qquad (38)$$

where the integration in (38) is along the open-sea boundary. The origin of the residual flow field within the basin is often a response to the net volume flux of water across the open-sea boundary that is generated by the mass transport in the primary forcing harmonic. This acts so as to lead to the fulfilment of (38). Ianniello [1981] has commented on a similar situation for the horizontally one-dimensional flow into a tidal channel.

The nonlinear terms supporting the residual circulation within the basin have been precisely identified by further experimentation with VIM. First, we omitted all the nonlinear advective flux terms from (30) and (31) and calculated the residual circulation by integration of the resulting equations. The pattern is both qualitatively and quantitatively indistinguishable from that given in Figure 5b. This indicates that the residual flow is supported either by the nonlinear bottom friction terms in (30) and (31) or possibly by the nonlinear shallow water terms implicit in (6). We next replaced the nonlinear friction terms by $-\lambda\bar{u}$ and $-\lambda\bar{v}$ where $\lambda \sim 10^{-3}$ m s^{-1}. In this case, computations showed that an identifiable residual circulation no longer exists; thus demonstrating the predominant role of the nonlinear bottom friction in determining the residual flow.

We may therefore conclude that the application of a fairly refined turbulence closure model leads to virtually the same results for the primary tidal and residual qualities as does a relatively simple depth-averaged model. This conclusion lends substantial support to the fairly widespread use of depth-averaged models in calculating residual circulations in shallow tidal seas.

4. Application to the Modeling of Wind-Driven Shallow Water Flow Over Topography

We consider in this section the application of (16) and (17) when the motion is driven by sea surface wind-stress forcing rather than by tidal forcing at the open-sea boundaries. To simplify

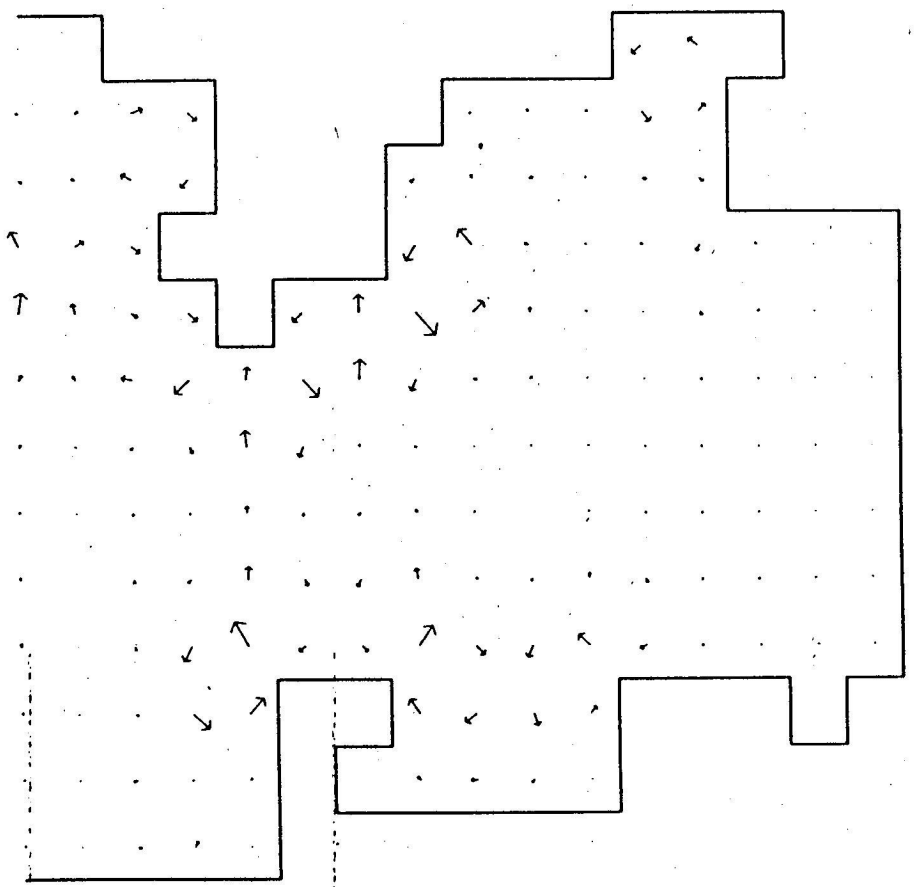

Fig. 5a. Depth-averaged residual velocity vectors calculated from MLM.

the computations, we consider first the case when the seafloor corresponds to $z = -h(x)$ and the analysis area is confined to $0 \leq x \leq L$. Prescribing that all dynamical conditions are independent of y, (6) reduces to

$$\frac{\partial \zeta}{\partial t} + \frac{\partial}{\partial x}(H\bar{u}) = 0 \tag{39}$$

Equations (16) and (17) reduce to

$$\frac{\partial \tilde{u}}{\partial t} + \frac{\partial}{\partial x}(u\tilde{u}) + \frac{\partial}{\partial \sigma}(\omega\tilde{u}) - f\tilde{v} = -gH\frac{\partial \zeta}{\partial x} + \frac{1}{H^2}\frac{\partial}{\partial \sigma}\left(K\frac{\partial \tilde{u}}{\partial \sigma}\right) \tag{40}$$

and

$$\frac{\partial \tilde{v}}{\partial t} + \frac{\partial}{\partial x}(u\tilde{v}) + \frac{\partial}{\partial \sigma}(\omega\tilde{v}) + f\tilde{u} = \frac{1}{H^2}\frac{\partial}{\partial \sigma}\left(K\frac{\partial \tilde{v}}{\partial \sigma}\right) \tag{41}$$

For consistency, the prescribed surface wind-stress $(\tau_x^\zeta, \tau_y^\zeta)$ must also be independent of y in which case there is no pressure gradient in the y-direction.

The turbulence energy density satisfies (20) with the omission of the advective flux term involving the y-derivative.

Lateral boundary conditions to be applied at $x = 0$ and $x = L$ are based upon the same type of radiative condition as used in Section 3. Specifically, we take

$$\bar{u} + \left(\frac{g}{h}\right)^{1/2}\zeta = 0 \quad \text{at } x = 0 \tag{42}$$

and

$$\bar{u} - \left(\frac{g}{h}\right)^{1/2}\zeta = 0 \quad \text{at } x = L \tag{43}$$

These equations form the basis for the numerical experiments to be performed on the wind-driven flow over an isolated topographical feature contained within $0 \leq x \leq L$. However, before discretizing these equations for numerical solution, it is necessary to apply a further coordinate transformation that will automatically lead to a finer resolution in the boundary layers adjacent to

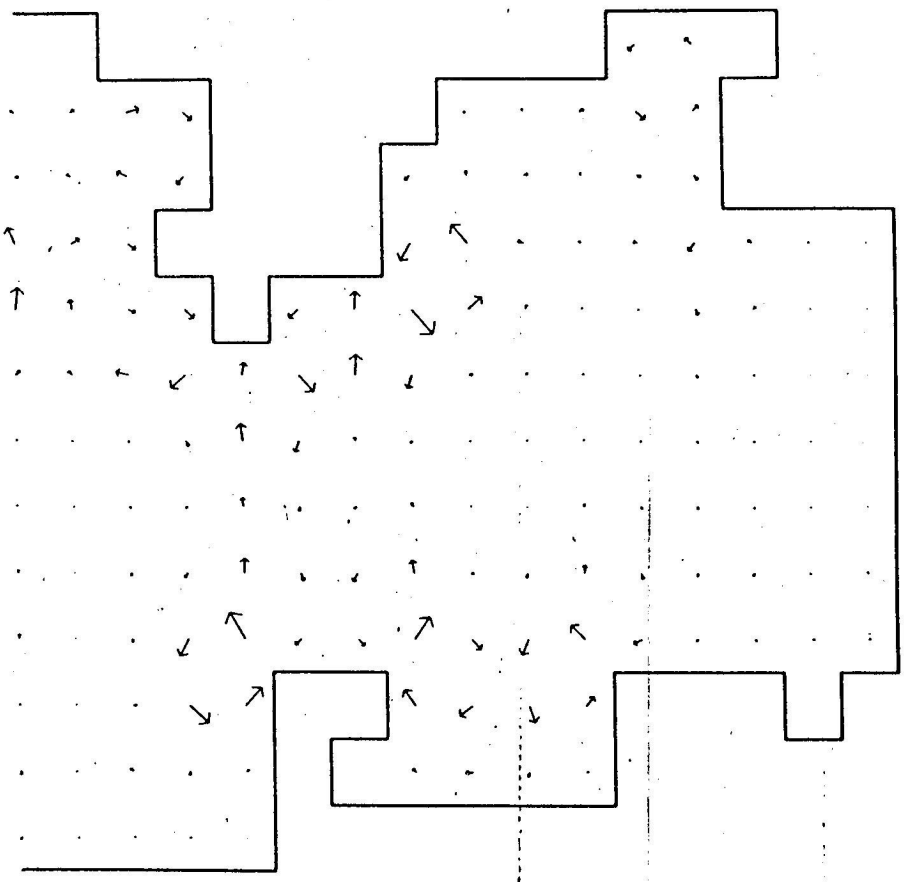

Fig. 5b. Same as Figure 5a except calculated from VIM.

both $\sigma = 0$ and $\sigma = 1$ as compared with the mid-depths. In section 3, a transformation was applied to obtain a finer resolution near $\sigma = 0$ compared with that near $\sigma = 1$. This is no longer good enough as the flow is now driven by a flux of momentum across the sea surface. This will lead to a boundary-layer structure near $\sigma = 1$ which must be adequately resolved. This transformation is described in detail by Johns et al. [1983].

In the numerical experiments, the length of the analysis region, L, is 40 km. The equilibrium depth is chosen according to

$$\frac{h}{h_0} = 1 \text{ for } |x - L/2| > L/4$$

$$\frac{h}{h_0} = 1 - \frac{1}{2}\sin\left[2\pi\left(\frac{x}{L} - \frac{1}{4}\right)\right] \text{ for } |x - L/2| < L/4 \qquad (44)$$

where $h_0 = 20$ m. Thus, there is a seafloor undulation consisting of a half-sinusoid of length 20 km. At the crest of this, the minimum equilibrium depth is 10 m. The maximum slope of the undulation is approximately 1.6×10^{-3}.

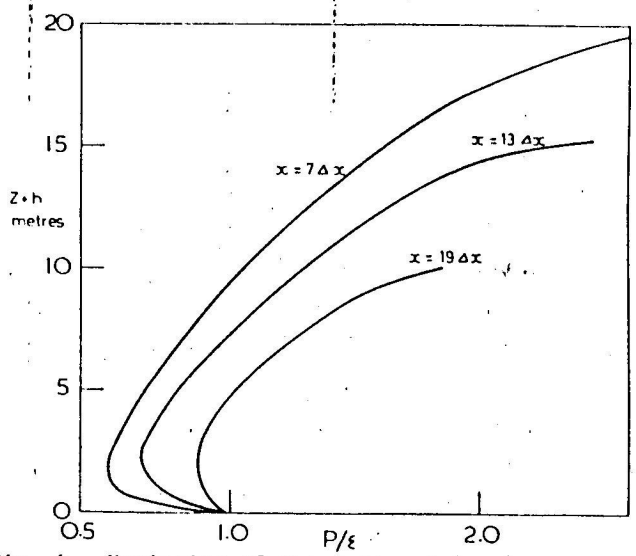

Fig. 6. Variation of the ratio of local turbulence production to dissipation as a function of height above the seafloor with $f = 0$ and $z_0 = 1$ cm at $x = 7\ \Delta x$, $13\ \Delta x$, and $19\ \Delta x$.

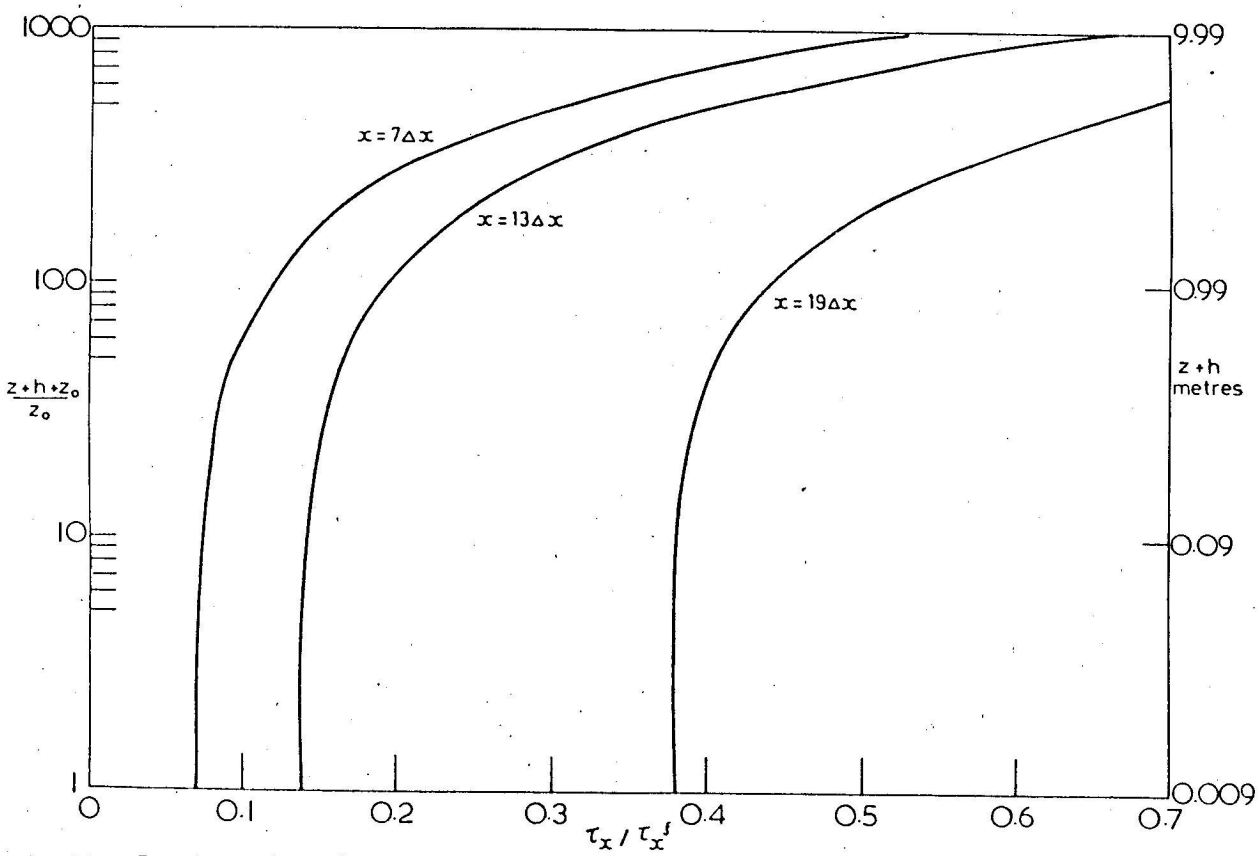

Fig. 7. Variation of the ratio of the internal stress to the applied surface stress as a function of height above the seafloor with f = 0 and z_0 = 1 cm at x = 7 Δx, 13 Δx, and 19 Δx.

A finite-difference grid is selected having 21 computational levels and with Δx = 1 km. The grid refinement implies that the first computational level above z = -h is between 5 and 10 mm above the seafloor. The first computational level below the free surface is at a depth of between 20 and 40 cm. The roughness length, z_0, is 1 cm, except where otherwise stated and, to obtain a significant response, a spatially and temporally uniform hurricane-strength wind-stress is applied for which .

$$\tau_x^\zeta = 4 \text{ Pa} \qquad \tau_y^\zeta = 0$$

With the prescribed forcing, the equations are integrated ahead in time from an initial state of rest. The integration is continued until the transient response is dissipated by friction thus leaving the steady state response to the uniform wind-stress forcing.

In the first experiment, f = 0, and the ensuing motion is strictly two-dimensional. Taking Δt = 1 min, the response attains an effectively steady state after about 2 hours of real time integration. In all the experiments, the flow parameters have been analyzed at three standard positions given by x = 7Δx, 13Δx, and 19Δx. These correspond to positions upstream of the undulation, on the slope of the undulation, and approximately at its crest. Denoting the production term in (12) by P, Figure 6 gives the variation of P/ε as a function of depth at these three positions. From this, it is seen that local production substantially exceeds dissipation in the upper half of the fluid because of the predominance of shear-generated turbulence resulting from the applied surface wind-stress. This excess of production over local dissipation is balanced by a down-gradient diffusion of turbulent energy to the lower half of the fluid where local dissipation exceeds shear-generated production. Production and dissipation are in approximate balance at mid-depths and, because of assumed local equilibrium conditions, at z = -h.

Figure 7 gives the variation of τ_x/τ_x^ζ through the fluid at each of the standard positions. At a height of about 1 m above the floor, it is seen that the deviation of τ_x from $\tau_{\underline{h}}^x$ is only about 5% of τ_x^ζ. Thus, there is an effective constant stress layer, having a thickness of about 1 m, above the seafloor. Above this layer, more substantial deviations of τ_x from $\tau_{\underline{h}}^x$ are seen to occur and, at 5 m above the floor, the departure lies between 23% and 28%. The higher percentage

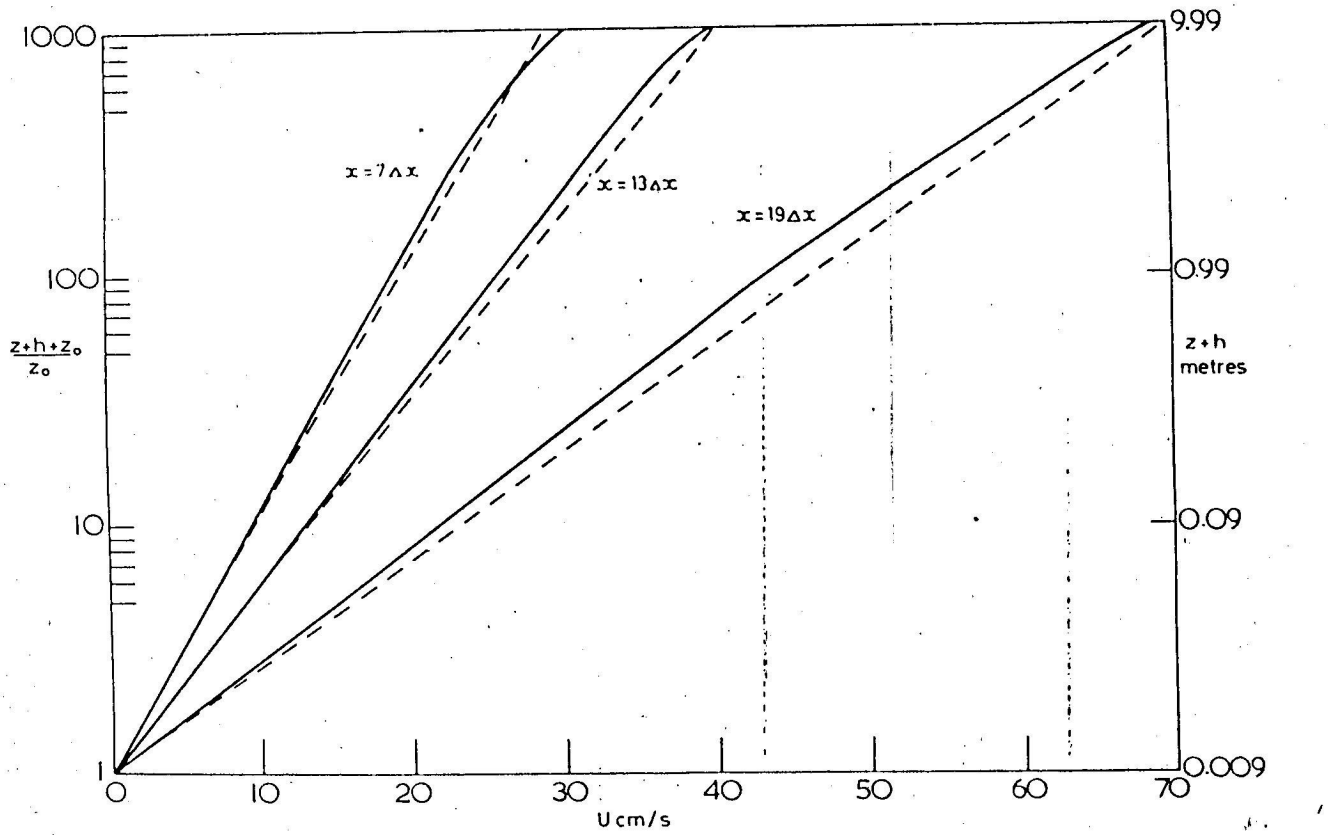

Fig. 8. Variation of the current velocity above the seafloor with f = 0 and z_0 = 1 cm at x = 7 Δx, 13 Δx, and 19 Δx.

deviation occurs, as is to be expected, at the crest of the undulation where the internal stresses are more strongly influenced by the applied surface stress.

The existence of an approximately constant stress layer above the seafloor suggests that the near-floor velocity profiles might be represented in terms of a logarithmic variation with height. Velocity profiles for the three standard positions are given in Figure 8. The logarithmic variation of these through the lowermost 1 m is apparent. The profiles (continuous curves) are compared with profiles (dotted curves) based on

$$u = \frac{u_*}{\kappa} \ell n \left(\frac{z + h + z_0}{z_0}\right) \qquad (45)$$

where

$$u_* = c^{1/4} E_b^{1/2} \qquad (46)$$

and E_b is the turbulent energy density at z = -h determined from the model. The excellence of the approximation through the lowermost 1 m is clear and, for x = 7Δx, (45) overestimates the model velocity by less than 3%. At x = 19Δx, this over-

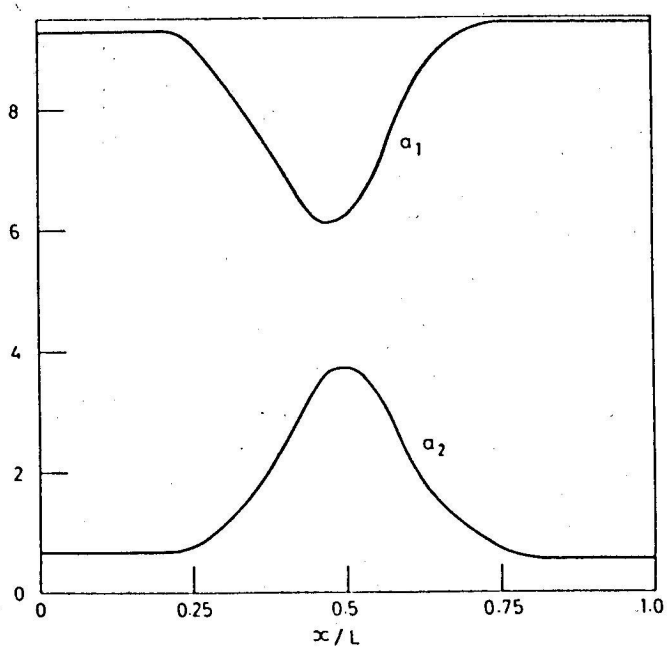

Fig. 9. Relative contribution of the pressure gradient term and the bottom stress term in the depth-averaged balance (47) with z_0 = 1 cm for 0 < x < L.

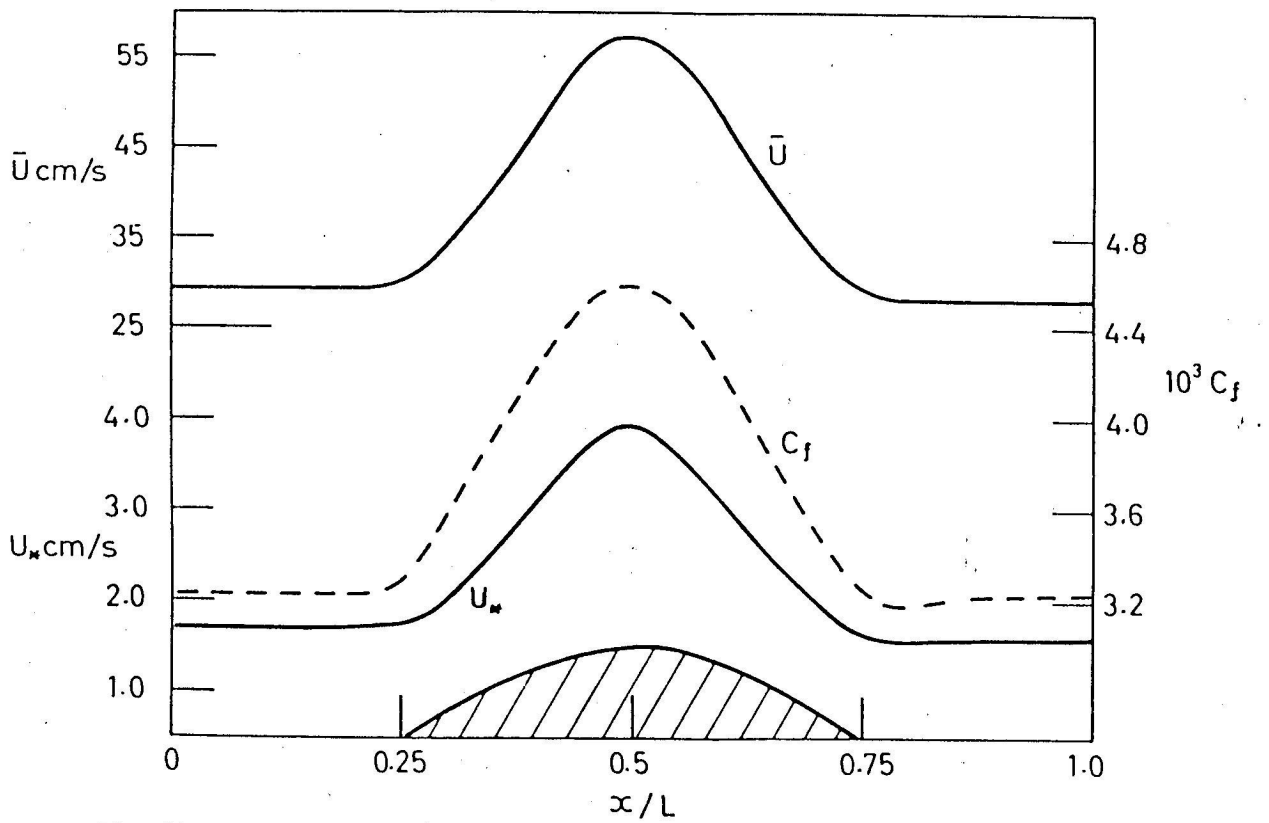

Fig. 10. Variation of the depth-averaged current, the bottom friction speed, and the friction coefficient with f = 0 and z_0 = 1 cm for $0 < x < L$.

estimation is increased to almost 7% which is consistent with the greater deviation of τ_x^{-h} from τ_x at the crest of the undulation.

In order to compare the terms in the dynamical balance, it is convenient to return to (40) with $\frac{\partial}{\partial t} = 0$ and f = 0. the depth-averaged balance then reduces to

$$\bar{u}\frac{\partial \bar{u}}{\partial x} + \frac{1}{(\zeta+h)}\frac{\partial}{\partial x}\,(\zeta+h)\,(\overline{u^2}) = -\,g\frac{\partial \zeta}{\partial x} + \frac{1}{\rho(\zeta+h)}\left(\tau_x^{\zeta} - \tau_x^{-h}\right) \quad (47)$$

The dominant terms in (47) are found to be the pressure gradient and the surface and bottom stresses. The relative importance of the pressure gradient and the bottom stress term to the surface stress term may be estimated by writing

$$a_1 = \frac{g(\partial\zeta/\partial x)(\zeta+h)}{(\tau_x^{\zeta}/\rho)} \quad (48)$$

$$a_2 = \tau_x^{-h}/\tau_x^{\zeta} \quad (49)$$

The variations of a_1 and a_2 for $0 < x < L$ are given in Figure 9. Upstream of the undulation, the bottom stress contributes only about 7% of the surface stress in (47) and there is a near-balance between the surface stress term and the pressure gradient. In the shallower water over the undulation, the contribution of the bottom stress becomes increasingly more important and, near the crest, accounts for some 37% in the balance. The contribution of the pressure gradient is then reduced to about 61% of the surface stress term. The remaining 2% is accounted for by the advective term in (47) with the second term on the left-hand side (the vertical structure correction term) making a negligible contribution. The advective term makes its greatest contribution at $x = 15\,\Delta x$ and $x = 25\,\Delta x$ where the slope of the undulation has its maximal effect. In these positions, it contributes 5% of the surface stress term in the depth-averaged balance.

The slope of the free surface varies between about 1.8×10^{-5} and 2.8×10^{-5} and leads to a difference in the surface elevation between x = 0 and x = L of about 80 cm.

In view of the frequent use made in storm surge modeling of empirically based representations of τ_x^{-h} in (47) having the form

$$\frac{\tau_x^{-h}}{\rho} = C_f \bar{u}^2 \quad (50)$$

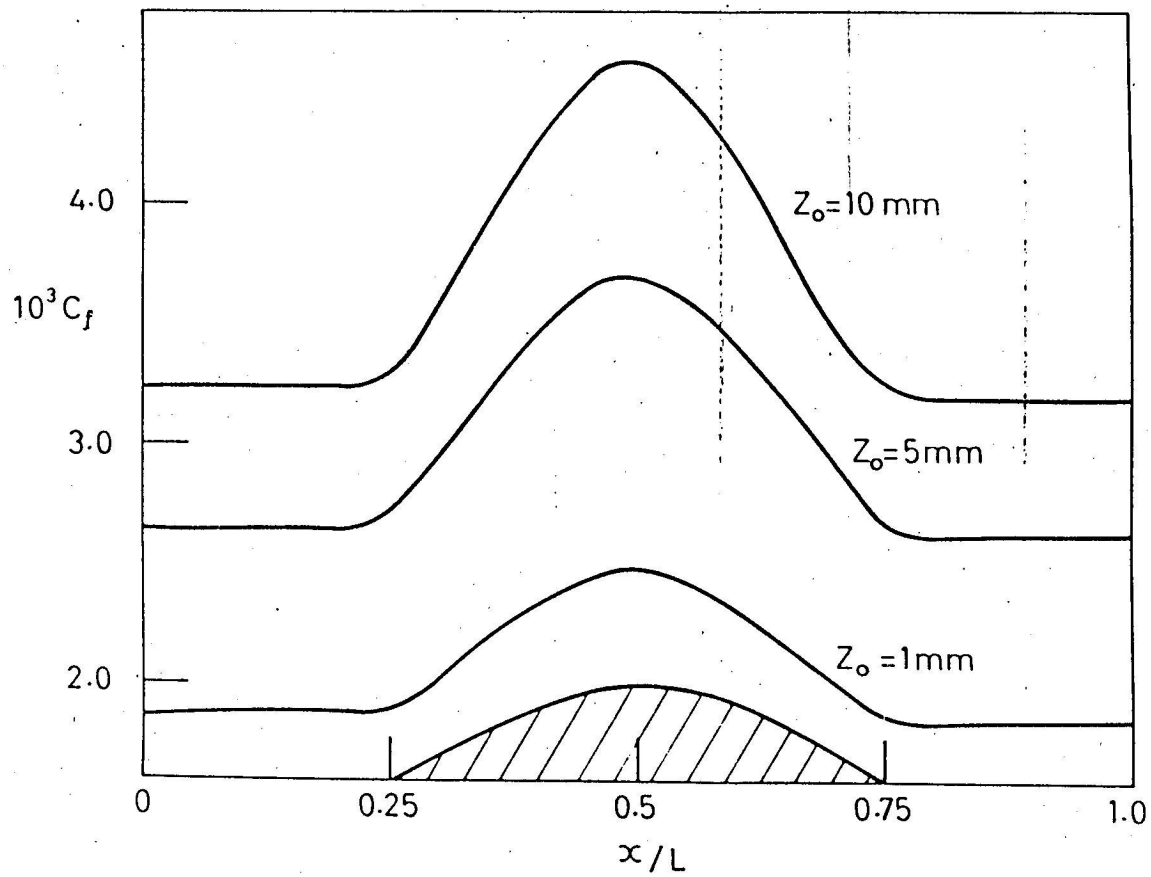

Fig. 11. Variation of the friction coefficient with f = 0 for $0 \leq x \leq L$ and with z_0 = 1 mm, 5 mm, and 1 cm.

where C_f is a friction coefficient, it is informative to consider the variation of u_*, $\bar{u}$, and C_f for $0 \leq x \leq L$. these are given in Figure 10, from which it is clear that both u_* and $\bar{u}$ peak over the crest of the undulation. the ratio $(u_*/\bar{u})$ is not, however, spatially uniform and C_f also shows a peaking at the crest of the undulation corresponding to an increase of about 43% over its upstream value.

Failure to take account of the spatial variability of C_f over irregular bottom topography may possibly lead to a serious misrepresentation of the bottom stress. In shallow water, where the bottom stress plays such an important role in the balance (47), this may have implications as regards the surge-induced sea surface elevation. For example, an overestimate of the bottom stress will imply increased frictional dissipation and a consequential underestimation of the surface elevation. In depth-averaged storm surge models, therefore, the neglect of the vertical structure correction term in (47) is probably justified but an appropriate parameterization of C_f may be required if the representation (50) is to be used.

The foregoing calculations have been performed with z_0 = 1 cm. However, C_f also has a dependence on the roughness length and its variation with z_0 is shown for $0 \leq x \leq L$ in Figure 11. For each of the three values considered, C_f shows a peaking over the undulation. With the lower roughness length of 1 mm, C_f increases by about 30% at the crest of the undulation over its upstream value. As previously stated, this compares with 43% for z_0 = 1 cm. With z_0 = 1 cm, the peak value of C_f is seen to be about 80% greater than the peak value for z_0 = 1 mm. These values of z_0 are certainly within the range encountered in shallow marine environments and the experiment indicates that the dependence of C_f on z_0 is of equal, if not greater importance, than its dependence on the local depth. For storm surge modeling, therefore, it would seem that C_f should also be parameterized in terms of z_0.

In the second experiment, the Coriolis acceleration is retained in the formulation and, in consequence, a transverse flow develops. Taking

$$f = 10^{-4} \text{ s}^{-1}$$

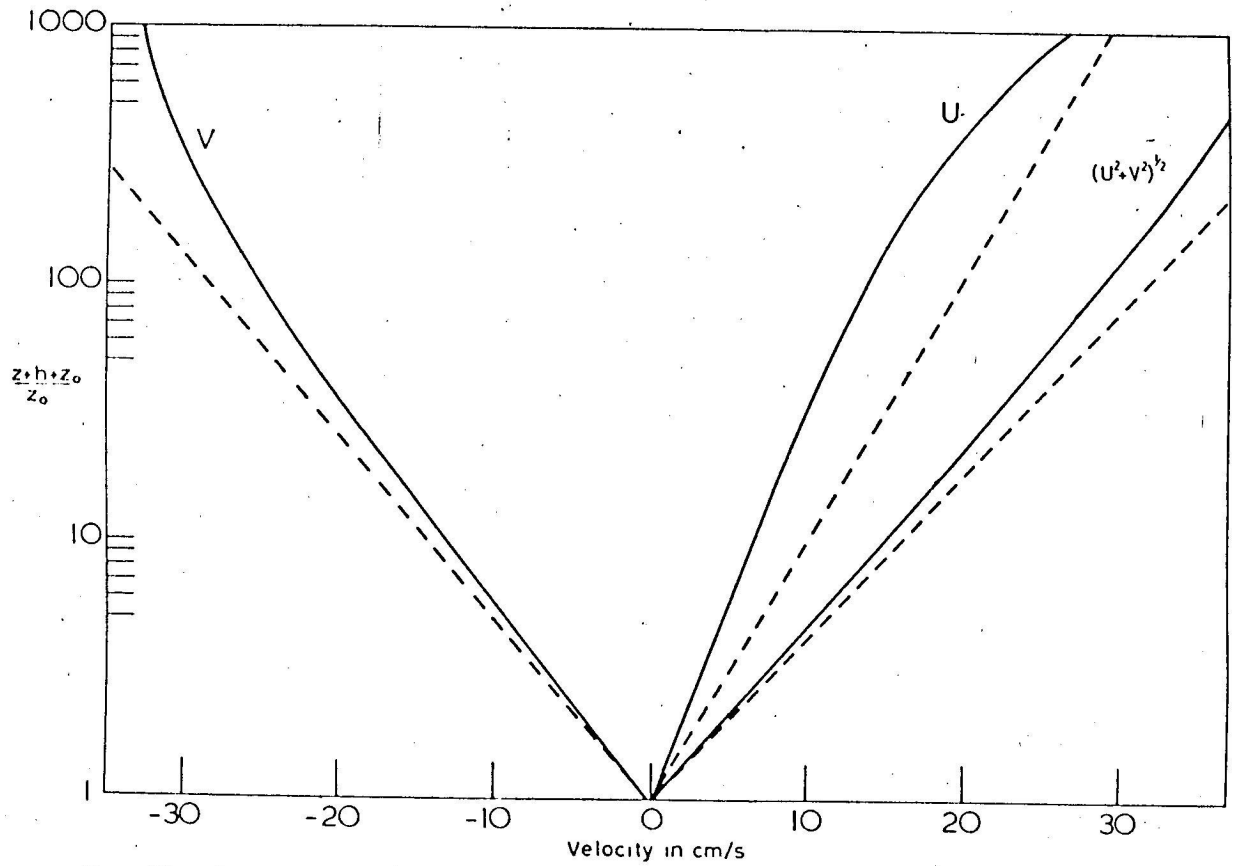

Fig. 12. Variation of the components of current and the current speed above the seafloor with $f = 10^{-4}$ s^{-1} and $z_0 = 1$ cm at $x = 7\,\Delta x$. Solid line is model profile and dashed line is constant stress profile.

and starting the integration from an initial state of rest, it is found that an effective steady state is reached after about 12 hours of real time. The longer period of integration (in comparison with that for $f = 0$) is required because of the development of an inertial oscillation in the response. The friction takes a longer time to dissipate the transitory component associated with this. With regard to the application of the approximate conditions (42) and (43), it is found that these introduce a localized distortion into the computed results adjacent to $x = 0$ and $x = L$. However, this only affects the first few grid-points from these end points and the results immediately upstream and downstream of the bottom undulation are uniform and entirely satisfactory.

In Figure 12, the variations of u and v at $x = 7\,\Delta x$ are given as a function of height above the seafloor. The near-logarithmic nature of these in a layer of thickness 1 m should be noted. It is also worthy of note that the surface current is in a direction 44° cum sole from the wind direction. With increasing depth, the angle of deflection increases and approaches 64° near the seafloor. Thus, the current vector is turned through an angle of about 20° between the free surface and the floor. The depth-averaged current is found to be in a direction of about 50° cum sole from the wind direction.

Also represented in Figure 12 is the variation with depth of the current speed $(u^2 + v^2)^{1/2}$. This quantity shows a logarithmic variation through the lowermost 1 m of the water and it is informative to compare this with an assumed constant stress logarithmic variation for the resultant current given by

$$(u^2 + v^2) = \frac{u_*}{\kappa} \ln \left(\frac{z + h + z_0}{z_0}\right) \qquad (51)$$

where u_* is now a friction speed given by

$$u_* = \left[\left(\frac{\tau_x}{\rho}\right)^{-h}_{2} + \left(\frac{\tau_y}{\rho}\right)^{-h}_{2}\right]^{1/4} \qquad (52)$$

Using (51), the current speed at a height of 1 m above the floor is found to be overestimated by

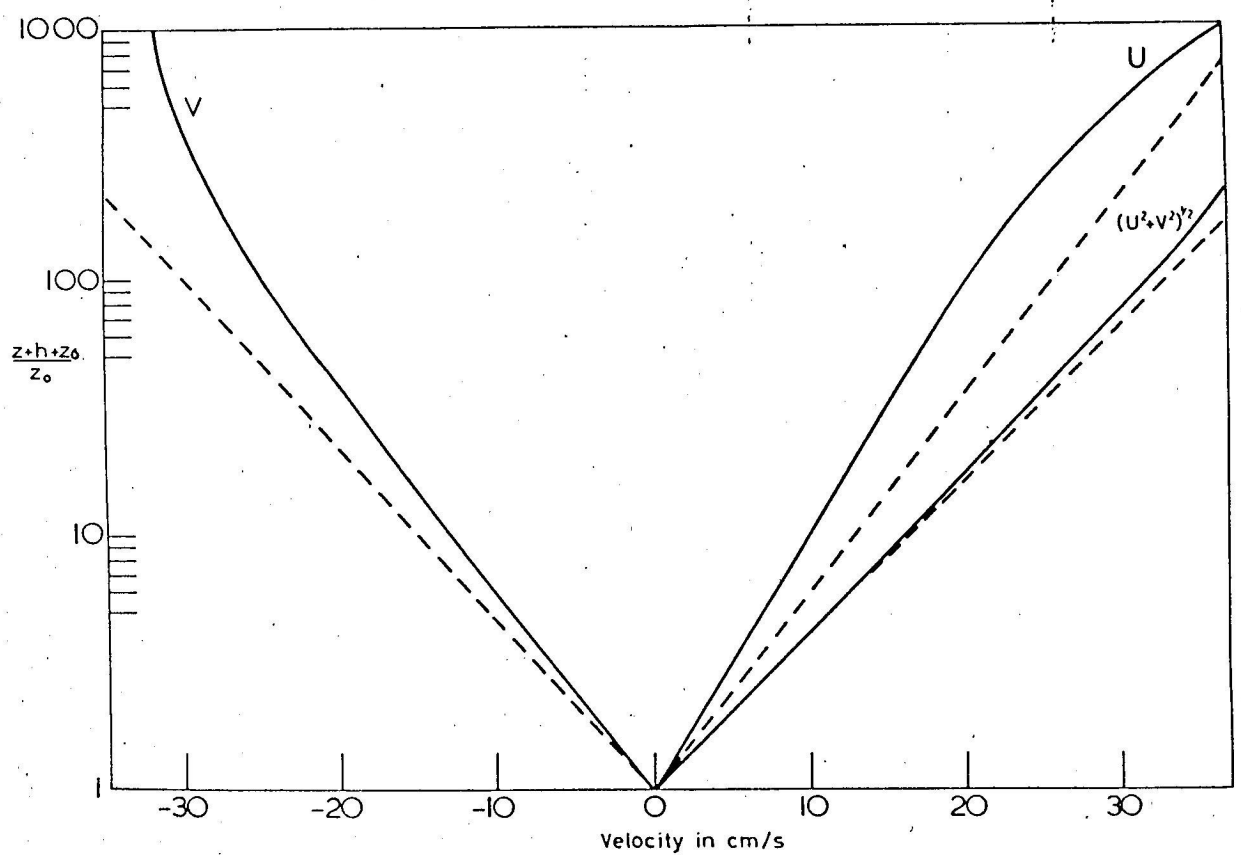

Fig. 13. Same as Figure 12 except that x = 13Δx.

about 10% as compared with 3% in the case with f = 0. It is also of interest to consider the possibility of representing u and v individually by

$$u = \frac{1}{\kappa}\left(\frac{\tau_x}{\rho}\right)^{1/2}\Big|^{-h} \ln\left(\frac{z+h+z_0}{z_0}\right) \qquad (53)$$

$$v = -\frac{1}{\kappa}\left(\left|\frac{\tau_y}{\rho}\right|\right)^{1/2}\Big|^{-h} \ln\left(\frac{z+h+z_0}{z_0}\right) \qquad (54)$$

Profiles based on (53) and (54) are also given in Figure 12 but it is seen, as might have been anticipated, that the model variation of u and v is not well-represented by these expressions. At a height of 1 m above the floor, the value of u is overestimated by as much as 44% while the magnitude of v is overestimated by about 14%.

In Figure 13, the same evaluations are given for x = 13 Δx. Here, the surface current is in a direction 37° cum sole from the wind direction while, near the floor, the angular deflection is about 53°. Thus, the shallower water has reduced the angle of turning between the surface and the floor to 16°. Within the lowermost 1 m, the current speed is approximated by (51) to within an accuracy of about 4% as compared with 10% at x = 7 Δx. This improvement is a result of the Coriolis acceleration inducing a smaller angle of turning between the free surface and the floor as the depth is reduced.

In Figure 14, the corresponding evaluations are given at x = 19 Δx. The angle of turning of the surface current relative to the wind direction is now reduced to 21° while that of the near-floor current is 28°. The current vector is therefore only turned through 7° between the surface and the floor and, within the lowermost 1 m of water, (51) now approximates the current speed to within an accuracy of less than 3%. It will also be noted that the representation of u by (53) improves as the depth of the water diminishes but the representation of v by (54) becomes worse.

An examination of the depth-averaged balance derived from (40), with $\partial/\partial t \equiv 0$, shows it to be very similar to the case with f = 0. The vertical structure correction term is again quite negligible and, upstream of the undulation, the Coriolis, the pressure gradient, and the bottom stress terms contribute respectively 17%, 75%, and 8% of

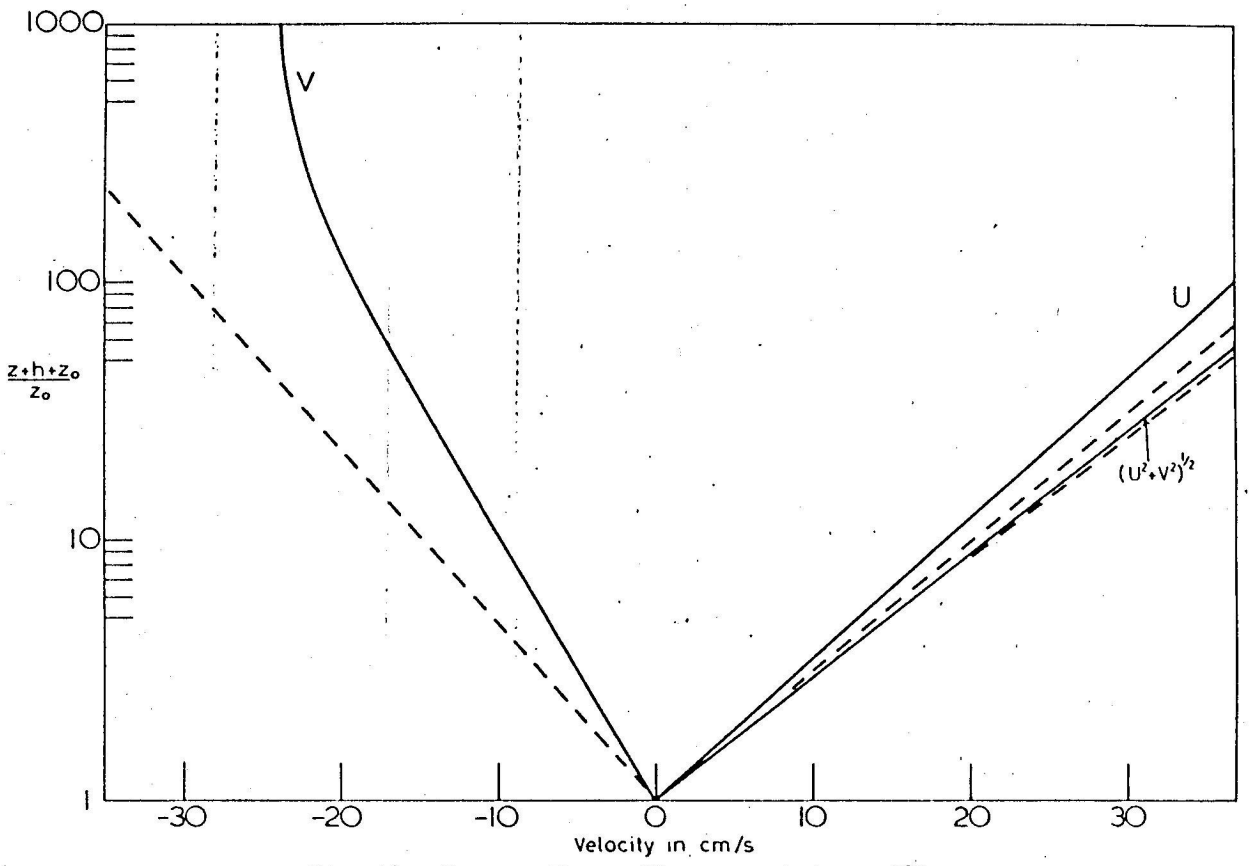

Fig. 14. Same as Figure 12 except that x = 19Δx.

the surface stress term. In the shallower water near the crest of the undulation, the contribution made by these terms becomes 6%, 63%, and 30%, with the horizontal advection term contributing about 1%. Thus, in this position, the bottom stress contribution is reduced in comparison with the case f = 0 and the balance is achieved through the Coriolis term.

The depth-averaged balance derived from (41) is essentially between the Coriolis term and the transverse bottom stress. Naturally, the transverse bottom stress term (but not necessarily the stress itself) attains its maximum value near the crest of the undulation where $\bar{u}$ is the maximum.

It remains to consider the effectiveness of the empirically based bottom friction to represent τ_x^{-h} and τ_y^{-h} defined in (8). Using (52) we can define a friction coefficient by

$$C_f = u_*^2/(\bar{u}^2 + \bar{v}^2) \qquad (55)$$

Thus, C_f is chosen to reproduce the magnitude of the bottom stress in terms of the speed of the depth-averaged current. At the three standard positions it is found that C_f has the values 4.16 x 10^{-3}, 4.17 x 10^{-3}, and 4.66 x 10^{-3}. It is then possible to consider the representation of the components of the bottom stress by

$$\frac{\tau_x^{-h}}{\rho} = C_f\,(\bar{u} + \bar{v})^{1/2}\,\bar{u} \qquad (56)$$

$$\frac{\tau_y^{-h}}{\rho} = C_f\,(\bar{u}^2 + \bar{v}^2)^{1/2}\,\bar{v} \qquad (57)$$

However, the effectiveness of this must be in some doubt since the direction of the bottom stress will not coincide with that of the depth-averaged current. In fact, at the three standard positions, τ_x^{-h}/ρ and τ_y^{-h}/ρ are respectively determined from the model (in $m^2\,s^{-2}$) to be 0.29 x 10^{-3}, 0.51 x 10^{-3}, 1.21 x 10^{-3}, and -0.61 x 10^{-3}, -0.67 x 10^{-3}, -0.66 x 10^{-3}. On the other hand, by using (56) and (57), these are approximated by 0.43 x 10^{-3}, 0.61 x 10^{-3}, 1.26 x 10^{-3} and -0.53 x 10^{-3}, -0.56 x 10^{-3}, -0.56 x 10^{-3}. thus, where the effect of the Coriolis acceleration is greatest, (56) overestimates the bottom stress by 48% and, where it is least, by about 4%. As far as the transverse bottom stress is concerned, (57)

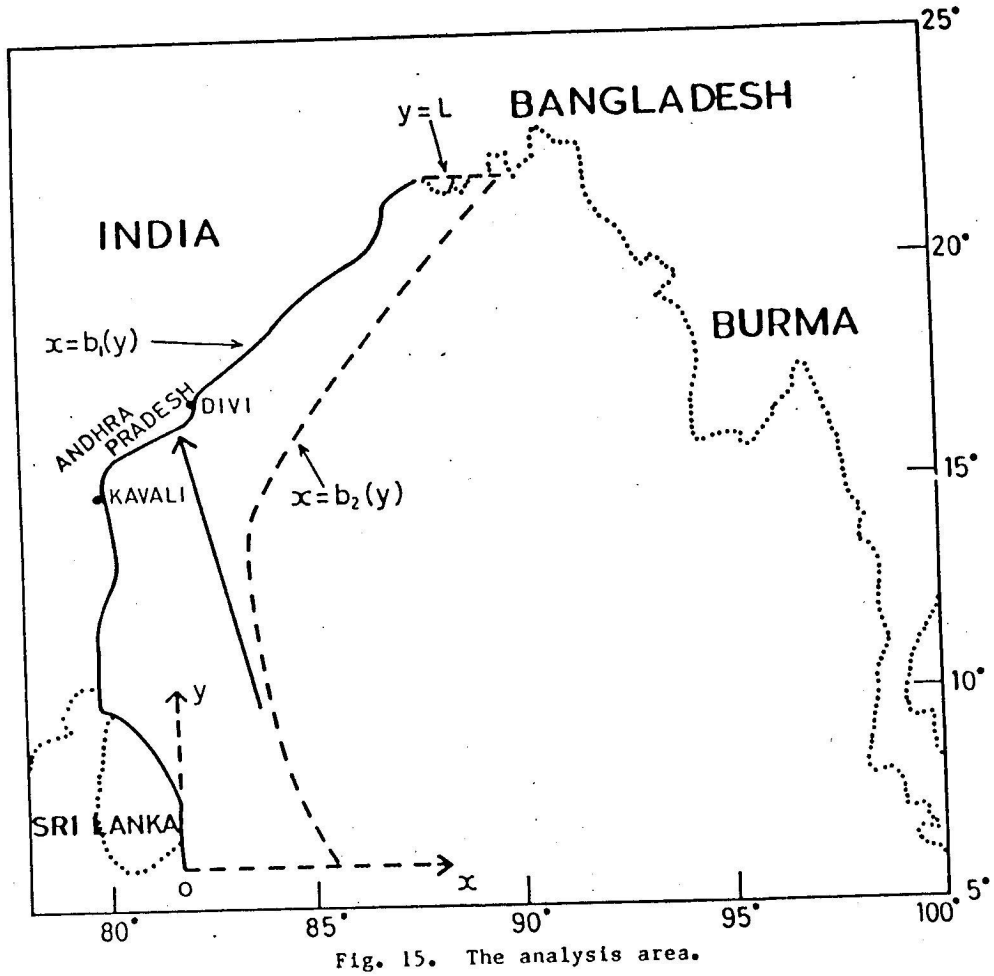

Fig. 15. The analysis area.

underestimates its magnitude by 21% upstream of the undulation and by 15% near the crest.

In conclusion, then, it appears that the empirical bottom stress representation given in (56) and (57) may be of questionable validity even if a parameterization of C_f can be made in terms of the local depth of water and the roughness length of the bottom elements. In the case of storm surge modeling, an estimate of the effect of using the empirical bottom stress representation is given in Section 5 by comparing the results of a numerical experiment based on the type of model considered here and one using a depth-averaged model.

5. Application to the Modeling of Storm Surges

The turbulence energy closure scheme has been applied by Johns et al. [1983] to the modeling of storm surges off the east coast of India. The full detail of this procedure is not reproduced here. It suffices to say that a further transformation of the x-coordinate is introduced by writing

$$\xi = \frac{x - b_1(y)}{b(y)} \tag{58}$$

where

$$b(y) = b_2(y) - b_1(y)$$

and $x = b_1(y)$ and $x = b_2(y)$ represent the eastern coastline of India and an eastern open-sea boundary. This configuration is shown in Figure 15. Thus, the coastline and open-sea boundary correspond respectively to $\xi = 0$ and $\xi = 1$. With ξ, y, σ, and t as new independent variables, it is shown by Johns et al. [1983] how the new coordinate system facilitates the numerical solution of the equations.

The surge is generated by an idealized cyclone which moves across the analysis area with a translation speed of between 13 and 14 km h^{-1}. Its initial position is centered about 1000 km southeast of the position of landfall and this corresponds to $t = 0$ when the system is at rest. The track is depicted in Figure 15.

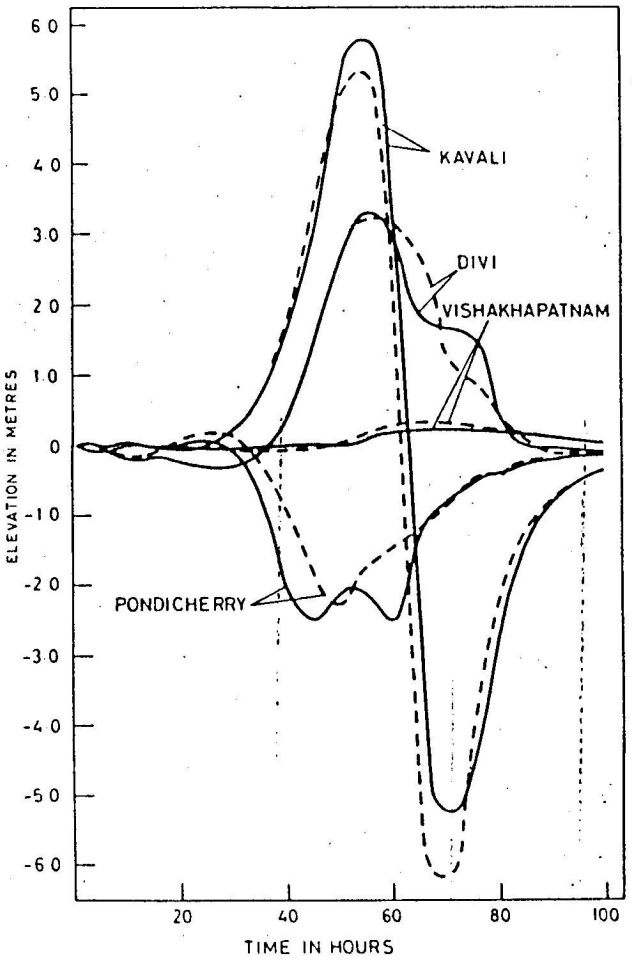

Fig. 16. Time variation of surface elevation at coastal stations. Solid line is computed from MLM, and dashed line is computed from DM.

With a wind-stress forcing calculated from an empirical representation of the wind speed in the cyclone, and with z_0 = 1 cm, we then computed from the model (now referred to as MML) the sea-surface elevation at the stations Vishkapatnam, Divi, Kavali, and Pondicherry whose geographical locations are described by Johns et al. [1981]. The responses have been compared with the corresponding sea-surface elevations determined from a depth-averaged model (DM) with $C_f = 2.6 \times 10^{-3}$. The results, shown in Figure 16, show a quite remarkable similarity. The differences that do exist are hardly significant although, compared with DM, we note a tendency for MLM to yield a higher positive surge at Kavali by approximately 9%. After the peak surge at Kavali, we note that both MLM and DM predict a rapidly falling sea-surface elevation with DM producing a greater peak negative surge than MLM by about 22%. We also note that the computed phase differences between MLM and DM are insignificant and that the peak elevations in the two models therefore occur at the same time.

It is important to consider this result in the light of our original expectation that the shallow water surge response calculated with MLM would be markedly different from that determined with DM. Firstly, why does the representation of the vertical current structure in MLM have such an insignificant effect on the results of the calculation? The application of DM is strictly admissible only when there is an absence of vertical current structure in a column of water. However, as pointed out in section 1, we would expect a vertical structure to evolve as momentum is transferred across the sea surface subsequently leading to motion at all depths. The key to answering the question lies in the fact that an evolving vertical current structure invalidates the depth-averaged equations used in DM only when the nonlinear momentum advection terms are of significant magnitude compared with the pressure gradient terms. This becomes increasingly the case in the shallow water adjacent to the coastline. However, the bulk of the momentum transfer from the atmosphere to the storm-induced currents takes place over the deeper water where the nonlinear advective terms are relatively unimportant. The developing surge response in the deeper water then propagates towards the coastal regions in the form of a long amplifying shallow water gravity wave. The coastal surge response is not locally generated but is produced by distant wind-stress forcing in regions where the existence of an evolving vertical current structure does not invalidate the use of the depth-averaged equations. Clearly, this argument may not apply in extensive shallow water regions where local generation must be expected to play a greater role. Such regions are to be found at the head of the Bay of Bengal where the possibility of a breakdown in the use of the depth-averaged equations must be recognized.

At first, we expected that our choice of value of z_0 would have an important effect on the computed surge response. The implication of such a result would be that a detailed knowledge of bottom roughness conditions is essential for incorporation into an effective storm surge model. Accordingly, we carried out a sequence of experiments in which z_0 was systematically varied between extreme plausible values. The results of this experimentation were illuminating and we found that the surge response with z_0 = 5 cm was virtually indistinguishable from that with z_0 = 1 cm.

Secondly, then, what is the reason for the relative insensitivity of MLM to variations in the bottom roughness? We expected that the surge response would be highly dependent on horizontal variations in z_0, these simulating varying seabed roughness conditions. That this is not the case must be attributed to the relative weakness of the

seabed friction in deep water compared with that in the shallow water coastal regions. Thus, the seabed roughness conditions in deep water are completely unimportant and, in our case, it appears that a value of z_0 lying between 1 cm and 5 cm is appropriate for the coastal regions where bottom friction is likely to be important.

References

Blumberg, A., and G. L. Mellor, in Mathematical Modelling of Estuarine Physics edited by J. Suendermann and J. P. Holz, 203-219, Springer-Verlag, Berlin, 1980.

Davies, A. M., Three-dimensional modelling of surges, in Floods Due to High Winds and Tides, edited by D. H. Peregrine, 45-74, Academic, Orlando, Fla., 1981.

Durance, J. A., A three-dimensional model of tidal motion in a shallow sea, Mem. Soc. R. Sci. Liege, Ser. 6, 10, 125-132, 1976.

Flather, R. A., and N. S. Heaps, Tidal computations for Morecambe Bay, Geophys. J. R. Astron. Soc., 42, 489-517, 1975.

Forristall, G. Z., Three-dimensional structure of storm-generated currents, J. Geophys. Res., 79, 2721-2729, 1974.

Freeman, N. G., A. M. Hale, and M. B. Danard, A modified sigma equations approach to the numerical modelling of Great Lakes hydrodynamics, J. Geophys. Res., 77, 1050-1060, 1972.

Heaps, N. S., A two-dimensional numerical sea model, Philos. Trans. R. Soc. London, Ser. A, 265, 93-137, 1969.

Heaps, N. S., On formulating a nonlinear numerical model in three dimensions for tides and storm surges, in Computing Methods in Applied Sciences, edited by R. Glowinski and J. L. Lions, p. 368-387, Springer-Verlag, Berlin, 1976.

Heaps, N. S. and J. E. Jones, Three-dimensional model for tides and surges with vertical eddy viscosity prescribed in two layers, II. Irish Sea with bed friction layer, Geophys. J. R. Astron. Soc., 64, 303-320, 1981.

Ianniello, J. P., Comments on tidally induced residual currents in estuaries: Dynamics and non-bottom flow characteristics, J. Phys. Oceanogr., 11, 126-134, 1981.

Jelesnianski, C. P. A numerical calculation of storm tides induced by a tropical storm impinging on a continental shelf, Mon. Wea. Rev., 93, 343-368, 1965.

Jelesnianski, C. P. Bottom stress time-history in linearized equations of motion for storm surges, Mon. Wea. Rev., 98, 462-478, 1970.

Johns, B., The modelling of tidal flow in a channel using a turbulence energy closure scheme, J. Phys. Oceanogr., 8, 1042-1049, 1978.

Johns, B., Numerical simulation of storm surges in the Bay of Bengal, in Monsoon Dynamics, edited by M. J. Lighthill and R. P. Pearce, 690-705, Cambridge University Press, New York, 1981.

Johns, B., and M. A. Ali, The numerical modelling of storm surges in the Bay of Bengal, Q. J. R. Meteorol. Soc., 106, 1-18, 1980.

Johns, B., S. K. Dube, U. C. Mohanty, and P. C. Sinha, Numerical simulation of the surge generated by the 1977 Andhra cyclone, Q. J. R. Meteorol. Soc. 107, 919-934, 1981.

Johns, B., P. C. Sinha, S. K. Dube, U. C. Mohanty, and A. D. Rao, Simulation of storm surges using a three-dimensional numerical model: an application to the 1977 Andhra cyclone, Q. J. R. Meteorol. Soc., 109, 211-224, 1983.

Koutitas, C. and B. A. O'Connor, Modeling three-dimensional wind-induced flows, Proc. J. Hydraul. Am. Soc. Civ. Eng. Div., 106, 1843-1865, 1980.

Launder, B. E. and D. B. Spalding, Mathematical models of turbulence, Academic, Orlando, Fla. 169 pp, 1972.

Leendertsee, J. J. and S. K. Liu, A three-dimensional turbulent energy model for non-homogeneous estuaries and coastal sea systems, in Hydrodynamics of estuaries and fjords, edited by J. C. J. Nihoul, pp. 387-405, Elsevier, New York, 1978.

Maddock, L. and R. D. Pingree, Numerical simulation of the Portland tidal eddies, Estuarine Coastal Mar. Sci., 6, 353-363, 1978.

Marchuk, I. G., V. P. Kochergin, V. I. Klimok, and V. A. Sukhorukov, On the dynamics of the ocean surface mixed layer, J. Phys. Oceanogr., 7, 865-875, 1977.

Nihoul, J. C. J., Three-dimensional model of tides and storm surges in a shallow, well mixed continental sea, Dyn. Atmos. Oceans, 2, No. 1, 29-47, 1977.

Nihoul, J. C. J., and F. C. Ronday, The influence of the "tidal stress" on the residual circulation: application to the Southern Bight of the North Sea, Tellus, 27, 484-489, 1975.

Nihoul, J. C. J., and F. C. Ronday, Hydrodynamic models of the North Sea, a comparative assessment, Mem. Soc. R. Sci. Liege, 10, 61-96, 1976.

Oguz, T., Numerical simulation of tidal circulation in oceanic basins and some related problems, Ph.D. thesis, 235 pp., University of Reading, Reading, England, 1981.

Phillips, N. A., A co-ordinate system having some special advantages for numerical forecasting, J. Meteorol., 14, 184-186, 1957.

Pingree, R. D., and L. Maddock, Tidal residuals in the English Channel, J. Mar. Biol. Assoc. U.K., 57, 339-354, 1977.

Prandle, D., Residual flows and elevations in the southern North Sea, Proc. R. Soc. London, Ser. A359, 189-228, 1978.

Reid, R. O., A. C. Vastano, R. E. Whitaker, and J. J. Wanstrath, Experiments in storm surge simulation, in The Sea, 6, edited by E. D. Goldberg, I. N. McCave, J. J. O'Brien, J. H. Steele, pp. 145-168. John Wiley, New York, 1977.

Ronday, F. C., Mesoscale effects of the tidal stress on the residual circulation of the North

Sea, Mem. Soc. R. Sci. Leige, Ser. 6, 7, 273-287, 1975.

Tee, K. T., Tide induced residual current, a 2-D nonlinear numerical tidal model, J. Mar. Res., 34, 603-628, 1976.

Tee, K. T., The structure of three-dimensional tide-induced current Part II: Residual currents, J. Phys. Oceanogr., 10, 2035-2057, 1980.

Vager, B. G., and B. A. Kagan, Vertical structure and turbulent regime in a stratified boundary layer of a tidal flow, Izv. Akak. Nauk SSSR Fiz. Atmos. Okeana, 7, 766-777, 1971.